THE FUNCTIONAL ROLE OF NEURAL OSCILLATORY ACTIVITY
IN PERCEPTION AND ACTION

By

YAN ZHANG

A DISSERTATION PRESENTED TO THE GRADUATE SCHOOL
OF THE UNIVERSITY OF FLORIDA IN PARTIAL FULFILLMENT
OF THE REQUIREMENTS FOR THE DEGREE OF
DOCTOR OF PHILOSOPHY

UNIVERSITY OF FLORIDA

2008

To my Dad, Mom and my husband, for their love and support

ACKNOWLEDGMENTS

TABLE OF CONTENTS

LIST OF FIGURES

LIST OF ABBREVIATIONS

ACC	Anterior cingulate cortex
AMVAR	Adaptive multivariate autoregressive
ANOVA	Analysis of variance
BESA	Brain electrical source analysis
CSD	Current source density
EEG	Electroencephalogram
ECoG	Electrocorticographm
ERP	Event-related potential
EMG	Electromyogram
EPSP	Excitatory postsynaptic potentials
fMRI	Functional magnetic resonance imaging
ICA	Independent component analysis
IPSP	Inhibitory postsynaptic potentials
ISI	Interstimulus interval
LFP	Local field potential
LORETA	Low resolution brain electromagnetic tomography
M1	Primary motor cortex
MEG	Magnetoencephalograpm
MPOs	Membrane potential oscillations
MUA	Multiple unit activity
N1	Middle-latency (~140 ms) evoked potential
PCA	Principle component analysis
PET	Positron emission tomography

PFC   Prefrontal cortex

PPC   Posterior parietal cortex

ROI   Region of interest

RT   Reaction time

S1   Primary somatosensory cortex

S2   Secondary somatosensory cortex

SCD   Scalp current density

SD   Standard deviation

SEM   Standard error of mean

SEP   Somatosensory evoked potential

sLORETA   Standardized low resolution brain electromagnetic tomography

SOBI   Second order blind identification

Abstract of Dissertation Presented to the Graduate School
of the University of Florida in Partial Fulfillment of the
Requirements for the Degree of Doctor of Philosophy

THE FUNCTIONAL ROLE OF NEURAL OSCILLATORY ACTIVITY
IN PERCEPTION AND ACTION

By

Yan Zhang

August 2008

Chair: Mingzhou Ding
Major: Biomedical Engineering

Spontaneous ongoing neural oscillations are traditionally considered to reflect an 'idling'

or deactivated brain state. In contrast, recent slice studies have demonstrated that the moderate

amount of membrane potential oscillations can bring the local neuron populations closer to the

firing threshold, making them more sensitive to a weak sensory stimulus. Other reports showed

that very high levels of spontaneous oscillations inhibit sensory evoked responses. Hence, to

distinguish these competing views, we investigated the relationship between ongoing neural

oscillations preceding stimulus presentation and subsequent cognitive processing and behavior.

First, we studied the relationship between reaction times and prestimulus neural

oscillations in a broad frequency band over multiple cortical regions. Second, we explored the

relationship between middle-latency somatosensory evoked potentials and prestimulus mu

oscillations. Third, we investigated the large-scale synchronization and directionality of

prestimulus neural activity in sensory perception and sensorimotor processing by applying

adaptive multivariate autoregressive coherence and Granger causality analysis.

In conclusion, our main findings suggest that cortical neural oscillations, especially

spontaneous ongoing neural oscillations, are crucial in subsequent cognitive perception and

behavioral performance. Also, the prestimulus neural synchronization over large-scale cortical

areas, play a key role in sensory processing and sensorimotor integration. For perception and action, these neural synchronizations help the top-down signals intrinsically generated from higher-order cortical regions (e.g., the prefrontal cortex) to interact with the bottom-up signals from lower-order cortical regions to facilitate the processing of forthcoming stimuli. These top-down attentional influences among multiple cortical regions are expected to play a functional role in selective processing of sensory input and motor output. Hence, this study suggests that spontaneous ongoing activity prior to stimulus onset may reflect an active not an idling brain state.

CHAPTER 1
INTRODUCTION

1.1 Background

Oscillatory neural activities have been widely observed in humans, nonhuman primates, and other mammalian species for several decades. These oscillations are conventionally described in terms of frequency bands, delta (1–3 Hz), theta (3–8 Hz), alpha (8–14 Hz), beta (14–30 Hz) and gamma (30–90 Hz). In recent years, new recording techniques have been widely applied to measure these neural oscillatory activities at high temporal and spatial resolutions. Examples include invasively-recorded local field potential (LFP) and electrocorticography (ECoG), as well as non-invasively recorded electroencephalogram (EEG), magnetoencephalogram (MEG), positron emission tomography (PET), and functional magnetic resonance imaging (fMRI). Particularly, LFP is an electrical signal of oscillatory neural activity from a population of cortical neurons located around electrodes, while scalp EEG or MEG measure a larger scale electrical neural activity, mostly like a superposition of LFPs. They have high temporal resolution (~ 1 ms), but low spatial resolution, while PET and fMRI have excellent spatial resolution but poor temporal resolution.

Spontaneous EEG signals were first robustly recorded from the human scalp in the mid-1920s by a psychiatrist (Berger, 1929). The first observed brain wave was termed the alpha (α) rhythm, mostly dominating in posterior regions. In healthy humans, the alpha rhythm has high-amplitude quasi-sinusoid waveforms during eye-closed rest and diminishes when the eyes are opened or under cognitive tasks. In addition, there are two more functionally distinct alpha-like rhythms. One occurring in pre- and post-central gyrus is called the mu rhythm (μ), sensitive to somatosensory stimuli and motor movement. The other generated above auditory cortical region is termed the tau (τ) rhythm, significantly blocked by acoustic stimulation. The alpha-like rhythm

is also found in prefrontal and other frontal cortices of healthy humans or during coma or anesthesia states (Nunez et al., 2001). The faster brain rhythm observed in sensorimotor and other frontal cortices is called the beta (β) rhythm, effectively associated with high-level stimulus processing and sensorimotor integration. The smallest-amplitude brain waveform, called the gamma (γ) rhythm, is often observed in primary sensory cortical areas.

These brain waves can be categorized as ongoing, evoked and induced oscillations. Ongoing oscillations indicate the spontaneous brain waves occurring before a stimulus or without any sensory stimulation. Evoked and induced oscillations both are referred to poststimulus events: evoked oscillations are phase-locked to stimulus onset and can be observed in average event related potentials, whereas induced oscillations can be cancelled out completely in this average approach.

These alpha-like rhythms and other band rhythms are believed to represent neural oscillations of postsynaptic potentials in neocortex (Nunez et al., 2001). At cellular levels, neurons in neocortex and other cortical structures have intrinsic membrane potential oscillations (MPOs), influencing the precise timing and integration of sensory input (Desmaisons et al., 1999; Bland et al., 2002; Vertes, 2005; Schaefer et al., 2006). These oscillatory activities are also determined by the intrinsic network organization and synchronization of the underlying neurons (da Silva, 1991). These intrinsic MPOs were found to synchronize over several centimeters and were also correlated with LFP (Nunez et al., 1987; Bland et al., 2002). Thus, these brain rhythms to some extent influence subsequent sensory and motor responses.

The brain rhythms are extensively explored in many research fields, including brain computer interface and cognitive neuroscience. Specially, scalp EEG signals are widely used in various clinical applications. Analyses of these rhythms have helped with clinical diagnosis of

various diseases, such as epilepsy, developmental disorders, movement disorder, autism, dementia and psychiatric diseases (da Silva, 1990). An increasing number of cutting-edge techniques help evaluate and analyze EEG signals, including power spectral analysis, independent component analysis (ICA), principle component analysis (PCA), second-order blind identification (SOBI), low resolution brain electromagnetic tomography (LORETA), and minimum-norm and beamforming algorithms.

1.2 Objectives

In cognitive neuroscience, an increasing number of studies support the idea that pre- or post-stimulus neural oscillations play significant roles in attention (Engel et al., 2001), anticipation (Brunia, 1999), associative learning (Miltner et al., 1999), movement maintenance (Conway et al., 1995; Brown, 2000; Brovelli et al., 2004), cognition and perception (Rodriguez et al., 1999). However, the underlying neural basis and functions of these neural oscillations are still in active debate.

In a classic view, ongoing spontaneous activity is considered 'background noise' and unrelated to subsequent stimulus processing. Specifically, the fact that spontaneous neural oscillations around 10-Hz and 20-Hz occur in the absence of stimuli or movement and are suppressed after stimulus appearance or during movement execution is taken as evidence that they reflect 'passive' or 'idling' brain states (Pfurtscheller et al., 1996b). Furthermore, these oscillations, specially alpha or alpha-like rhythms, are thought to reflect the top-down inhibitory control of cortical stimulus processing because they strengthen during memory retention, implying the block of item retrieval, and diminish during memory retrieval (Klimesch et al., 2007).

However, these two hypotheses have been challenged by recent studies (Arieli et al., 1996; Destexhe and Pare, 1999; McCormick et al., 2003; Shu et al., 2003; Linkenkaer-Hansen et

15

al., 2004), which suggest that spontaneous oscillatory activity may reflect a depolarizing drive to local neuron populations and bring them closer to firing threshold, thereby facilitating the sensory detection of weak sensory input. Thus, the absence or lack of spontaneous activity results in small sensory responses. However, the extreme high level of spontaneous ongoing oscillations has been also found to inhibit not enhance cortical sensory processing by competing with sensory evoked responses (Petersen et al., 2003; Dehaene and Changeux, 2005).

Classical theories postulated that the brain is a passive system, determined by external stimuli. However, recent studies (Engel et al., 2001) suggest that the brain is an active and adaptive system and the internal brain states influence stimulus information processing. Top-down signals, which reflect states of attention and anticipation, intrinsically generated from higher-order cortical regions, interact with bottom-up signals generated from lower-order cortical regions to create an optimal brain state and thus facilitate sensory responses.

The highest level of this cortical hierarchy is the prefrontal cortex, located in the anterior part of the frontal lobe. Anatomical evidence and numerous physiological studies (Fuster, 2001) suggest that the prefrontal cortex mediates top-down control by sending excitatory and inhibitory 'bias signals' to lower-order sensorimotor circuits. Conversely, the primary sensory cortices, including visual, auditory, and somatosensory cortex, are believed to be the low order cortical regions.

The top-down control is found to be mediated by corticocortical synchronization in both ongoing and evoked neural activity. A great deal of research focuses on the functional significance of neural synchronization during stimulus processing. However, ongoing neural activity preceding the presentation of stimulus, reflecting anticipation and prediction of forthcoming sensory and motor events, attracts increasing interest (Arieli et al., 1996; Kastner et

al., 1999; Tsodyks et al., 1999; Engel et al., 2001; Dehaene and Changeux, 2005). It is suggested that the intrinsic bias signals from high-order cortical areas might create a facilitatory brain state conducive to subsequent stimulus processing.

Hence, this research investigates the relationship between spontaneous ongoing oscillations and sensorimotor processing along three specific aims.

- Investigate the relationship between prestimulus neural oscillations over multiple cortical regions and the speed of visuomotor processing.

- Investigate time-frequency features and network connection characteristics of cortical sensorimotor oscillations in a visuomotor discrimination task.

- Investigate the relationship between prestimulus mu oscillations in the sensorimotor cortex and the N1 component, which is a middle-latency somatosensory evoked potential component, in a somatosensory perception experiment and test the hypothesis that the top-down attentional control facilitates subsequent sensory perception.

CHAPTER 2
GENERAL METHODS

The main analysis techniques applied in the present study are: adaptive multivariate

autoregressive (AMVAR) power and coherence spectral analysis, Granger causality spectral

analysis and conditional Granger causality analysis.

2.1 Adaptive Multivariate Autoregressive Spectral Analysis

Adaptive multivariate autoregressive modeling is a parametric spectral analysis method

in which time series models are adaptively extracted from the dataset having a number of

realizations (Ding et al., 2000). The fundamental assumption of this algorithm is that the short-

window time series can be treated as realizations of an underlying stationary stochastic process.

As cognitive information processing changes rapidly, AMVAR can be used to investigate the

time series in a short window size (< 100 ms). The following is the procedure of AMVAR.

Let $X(t)$ be a p-dimensional stationary random process $[X(1,t), X(2,t), \ldots, X(p,t)]^T$.

$X(t)$ can be modeled by the autoregressive equations (Equation 2-1). Here $A(i)$ are the

unknown $p \times p$ coefficient matrices where $i = 1, 2, \cdots, m$, $E(t)$ is the zero-mean uncorrelated

noise term with covariance matrix Σ, and m is the model order.

$$X(t) + A(1)X(t-1) + A(2)X(t-2) + \cdots + A(m)X(t-m) = E(t) \qquad (2\text{-}1)$$

We multiply $X^T(t-k)$, where $k = 1, 2, \cdots, m$, to Equation 2-1 and take expectation on

both sides to acquire the Yule-Walker equations. $R(j)$ are the covariance matrices of

$X(t)X^T(t+j)$ with lag j. Coefficient matrices $A(i)$ and covariance matrix Σ of noise term

$E(t)$ are obtained by solving Equation 2-2 through the Levinson, Wiggins and Robinson (LWR)

algorithm (Morf et al., 1978).

$$R(-k) + A(1)R(-k+1) + \cdots + A(m)R(-k+m) = 0 \tag{2-2}$$

Spectral features are derived from AMVAR models after acquiring $A(i)$ and Σ estimates. Equation 2-1 can be written in a spectral domain equation (Equation 2-3). The spectral transform $X(f)$ can be obtained by dividing $A(f)$ on both sides of Equation 2-3 and define $H(f)$ as a transfer matrix.

$$A(f)X(f) = E(f) \tag{2-3}$$

$$X(f) = H(f)E(f) \tag{2-4}$$

$$H(f) = \left(\sum_{i=0}^{m} A(i)e^{-ij2\pi f} \right)^{-1} \tag{2-5}$$

Thus, spectral power $S(f)$ can be obtained through Equation 2-6. The symbol '*' means both transpose and complex conjugate. Spectral power is contained in the diagonal terms of the spectral matrix. Coherence spectra between two random process $X(i,t)$ and $X(j,t)$ is defined as $C(f)$. If the coherence value is equal to 1 or 0, the two processes are maximally interdependent or independent, respectively. Here the autoregressive model order is determined by minimizing the Akaike Information Criterion (AIC).

$$S(f) = \lim_{N \to \infty} \frac{1}{N} E[X(f)X^*(f)] = H(f)\Sigma H^*(f) \tag{2-6}$$

$$C_{ij}(f) = \frac{\left| S_{ij}(f) \right|^2}{S_{ii}(f)S_{jj}(f)} \tag{2-7}$$

$$AIC(m) = -2\log[\det(\Sigma)] + \frac{2mp^2}{N} \tag{2-8}$$

2.2 Granger Causality Analysis

Granger causality is a key technique to assess the directionality of neural communications. Multivariate autoregressive modeling provides a natural and useful framework for incorporating the computation of Granger causality. The fundamental idea of Granger causality is that if the better prediction of one time series $X(t)$ could be achieved by including the past measurement of time series $Y(t)$, $Y(t)$ is said to have a causal influence on $X(t)$.

2.2.1 Pairwise Analysis

Given two stochastic processes X_t and Y_t and assuming they are jointly stationary, X_t can be represented by linear autoregressive models. Here ε_n is a gauge of the prediction accuracy and η_n is a gauge of the prediction accuracy of the new expanded predictor. The covariance matrix of the noise term is Σ.

$$
\begin{aligned}
X_n &= a_1 X_{n-1} + \cdots + a_m X_{n-m} + \varepsilon_n \\
X_n &= b_1 X_{n-1} + \cdots + b_k X_{n-k} + c_1 Y_{n-1} + \cdots + c_k Y_{n-k} + \eta_n
\end{aligned}
\tag{2-9}
$$

$$
\Sigma = \begin{pmatrix} \Sigma_{11} & \Sigma_{12} \\ \Sigma_{21} & \Sigma_{22} \end{pmatrix}
\tag{2-10}
$$

Granger (Granger, 1969) formulated that, if variance of η_n is less than that of ε_n, namely $\dfrac{Var(\eta_n)}{Var(\varepsilon_n)} < 1$, $Y(t)$ is said to have a causal influence on $X(t)$. Geweke (Geweke, 1982; Ding et al., 2006) showed that, the total linear interdependence $F_{X,Y}$ between two time series $X(t)$ and $Y(t)$ can be decomposed into three components $F_{X \to Y}$, $F_{Y \to X}$, and $F_{X.Y}$. Here $F_{X \to Y}$ and $F_{Y \to X}$ are the causal influences due to their intrinsic interaction patterns. $F_{X \to Y}$ is a measure of the linear directional influence from $X(t)$ to $Y(t)$. Similarly, $F_{Y \to X}$ is a measure of the return

influence from $Y(t)$ to $X(t)$. $F_{X.Y}$ is the instantaneous causality due to factors possibly

exogenous to the (X,Y) system (e.g., a common driving input) .

$$F_{X,Y} = F_{X \to Y} + F_{Y \to X} + F_{X.Y} \tag{2-11}$$

Geweke demonstrated that the measures of Granger causality in time domain could be

decomposed into their frequency content. F is defined as Granger causality in time domain and

$I(f)$ is defined as Granger causality spectrum.

$$F_{Y \to X} = \frac{1}{2\pi} \int I_{Y \to X}(f) df \tag{2-12}$$

Each of the above time domain quantities is defined in the following equations. C(ω) is

the coherence function and $\omega = 2\pi f$.

$$F_{X,Y} = \frac{1}{2\pi} \int_{-\pi}^{\pi} \ln(1 - C(\omega)) d\omega \tag{2-13}$$

$$F_{X \to Y} = \frac{1}{2\pi} \int_{-\pi}^{\pi} I_{X \to Y}(\omega) d\omega \tag{2-14}$$

$$F_{Y \to X} = \frac{1}{2\pi} \int_{-\pi}^{\pi} I_{Y \to X}(\omega) d\omega \tag{2-15}$$

$$F_{X.Y} = \frac{1}{2\pi} \int_{-\pi}^{\pi} I_{X.Y}(\omega) d\omega \tag{2-16}$$

$$C(\omega) = \frac{|S_{12}(\omega)|^2}{S_{11}(\omega) S_{22}(\omega)} \tag{2-17}$$

After some algebraic derivation, the Granger causality spectrum from one time series

$X_1(t)$ to the other one $X_2(t)$ is expressed as:

$$I_{1 \to 2}(f) = -\ln(1 - \frac{(\Sigma_{11} - \frac{\Sigma_{12}^2}{\Sigma_{22}})|H_{21}(f)^2|}{S_{22}(f)}) \tag{2-18}$$

Similarly, the Granger causality spectrum from $X_2(t)$ to $X_1(t)$ is:

$$I_{2 \to 1}(f) = -\ln(1 - \frac{(\Sigma_{22} - \frac{\Sigma_{12}^2}{\Sigma_{11}})|H_{12}(f)^2|}{S_{11}(f)})$$

(2-19)

Here $S_{ii}(f)$ is the power spectra of $X_i(t)$.

2.2.2 Conditional Granger Causality Analysis

For multiple time series, the aforementioned pairwise analysis is unable to reflect the true casual patterns due to mediated causal influences. Conditional Granger causality analysis (Chen et al., 2006; Ding et al., 2006) is defined to resolve whether the interaction between two time series is direct or is mediated by a third process.

Given three stochastic processes X_t, Y_t and Z_t, their joint representation is given by the following linear models:

$$X_n = \sum_j d_j X_{t-j} + \sum_{j=1}^{\infty} e_j Y_{t-j} + \sum_{j=1}^{\infty} g_j Z_{t-j} + \varepsilon_t$$

$$Y_n = \sum_{j=1}^{\infty} k_j X_{t-j} + \sum_{j=1}^{\infty} m_j Y_{t-j} + \sum_{j=1}^{\infty} n_j Z_{t-j} + \eta_t$$

(2-20)

$$Z_n = \sum_{j=1}^{\infty} u_j Z_{t-j} + \sum_{j=1}^{\infty} v_j Y_{t-j} + \sum_{j=1}^{\infty} w_j Z_{t-j} + \gamma_t$$

The covariance matrix of the noise terms is:

$$\Sigma = \begin{pmatrix} \Sigma_{xx} & \Sigma_{xy} & \Sigma_{xz} \\ \Sigma_{yx} & \Sigma_{yy} & \Sigma_{yz} \\ \Sigma_{zx} & \Sigma_{zy} & \Sigma_{zz} \end{pmatrix}$$

(2-21)

The Granger causality from Y_t to X_t conditional on Z_t is defined to be:

$$F_{Y \to X|Z} = \ln \frac{\Sigma_{11}}{\Sigma_{xx}}$$

(2-22)

If the causal influence from Y_t to X_t is completely mediated by Z_t, $\Sigma_{11} = \Sigma_{xx}$ and $F_{Y \to X | Z} = 0$. The spectral representation of conditional Granger causality has also been developed and will be used in this study.

CHAPTER 3
ONGOING OSCILLATIONS AND VISUOMOTOR PROCESSING SPEED

3.1 Introduction

Oscillatory neural activity has been widely observed in nonhuman primates and humans. Alpha and gamma oscillations are characteristics of the primate visual systems (Vanessen and Gallant, 1994), while Beta (15–30 Hz) oscillations were prevalent in local field potentials of the primate sensorimotor and parietal cortices (Sanes and Donoghue, 1993; MacKay and Mendonca, 1995). These neural oscillations are believed to be associated with neural communications and to some extent be correlated with the human brain rhythms. However, the underlying neural mechanism of these neural oscillations is still unclear.

The classical notion of neural activities in the alpha and low beta (8–20 Hz) bands is that they represent an 'idling' state of the brain (Pfurtscheller et al., 1996b). The main evidence is that the alpha and low beta activity is diminished with attentional demand whereas the high beta band activity is enhanced in cognitive processing (Ray and Cole, 1985). Also, alpha oscillations have been proposed to reflect the spatially-specific disengagement of visual anticipatory attention (Foxe et al., 1998). On the other hand, alpha band rhythm has been reported to be a sign of good cognitive and memory performance (Klimesch, 1999). Likewise, cortical beta activity has been reported to be associated with states of vigilance, attention to sensorimotor integration (Murthy and Fetz, 1992) or maintenance of a precise motor force or limb position (MacKay and Mendonca, 1995; Brovelli et al., 2004). These conflicting views about these alpha and beta oscillations may stem from different experimental paradigms and different analysis strategies employed in various studies. A uniform design in conjunction with standardized analysis holds the key to resolve these conflicts.

Reaction time (RT) measures the overall efficacy of cognitive and sensorimotor processing. RT is known to exhibit considerable variability from trial to trial, which is thought to reflect the spontaneous fluctuation of the subject's state of expectancy and attention, with faster RT arising from a more alert and attentive state. Theoretically, the fluctuation of RT is often modeled from the perspective of stimulus-driven information processing. Recent work has begun to examine how cortical activity prior to stimulus presentation impacts subsequent visuomotor performance. In light of the fact that various oscillatory population activities have been shown to mediate important cortical functions, such as anticipation of forthcoming stimuli and motor preparation (Brunia, 1999; Engel et al., 2001; Varela et al., 2001), it raises the question of whether and how spontaneous ongoing oscillatory cortical activity affects RT.

Previous studies (Donchin and Lindsley, 1966; Morrell and Morrell, 1966; Haig and Gordon, 1998; Gonzalez Andino et al., 2005) have demonstrated that specific components of EEG and MEG, for example, ERP amplitude and spectral power, are correlated with RT. Specially, it has been suggested that prestimulus neural activity is significantly correlated with motor performance (Winterer et al., 1999; Liang et al., 2002; Linkenkaer-Hansen et al., 2004; Gonzalez Andino et al., 2005). Liang et al. (2002) showed that prestimulus beta power in the prefrontal cortex was negatively correlated with RT. Winterer et al. (1999) demonstrated that increased prestimulus delta-band EEG signals in frontal cortical areas, reflecting increased cortical activation, were significantly correlated with faster RT.

However, many previous reports of prestimulus activity have been basically limited in two key aspects. First, due to common reference and volume conduction, studies based on human scalp EEG/MEG have methodological difficulties to localize the underlying neural generators. The relatively poor spatial resolution results in inability to study brain functions in

25

specific brain systems. Second, data analysis has been often confined to a single predefined frequency band, which prevents the investigation of oscillatory interaction between different frequencies.

In the present study, to overcome these problems, we analyzed simultaneous LFPs from up to sixteen cortical recording sites distributed broadly over one hemisphere in three macaque monkeys trained to perform a visuomotor pattern discrimination task. The relation between prestimulus LFP activity and RT was examined across a broad range of frequencies and cortical regions.

3.2 Materials and Methods

3.2.1 Paradigm and Data Acquisition

Experiments were performed at the Laboratory of Neuropsychology at National Institute of Mental Health (NIMH). Animal care was in accordance with the institutional guidelines at that time. The LFPs data, called the Nakamura dataset, were simultaneously recorded from multiple surface-to-depth bipolar teflon-coated platinum electrodes chronically implanted in one cerebral hemisphere of three highly trained macaque monkeys performing a visual-motor pattern discrimination task. The data were analog filtered (-6 dB at 1 and 100 Hz, 6 dB per octave falloff) and digitized at 200 samples/s.

The monkeys initiated each trial by depressing and holding steadily a lever with their preferred hand. Visual stimuli randomly appeared after the beginning of each trial and stayed on a display screen for 100 ms. The visual stimulus onset was defined as 0 ms. Each visual stimulus consisted of four dots arranged as a (left- or right-slanted) diamond or line. Monkeys responded (GO conditions) to one visual pattern type (line or diamond), and withheld responding (NO-GO conditions) to the other.

Data collection began about 90 ms preceding the presentation of visual stimuli and continued until 505 ms post-stimulus. On GO trials, the monkey received a water reward at 505 ms post-stimulus if the hand was lifted within 500 ms. On NO-GO trials, the lever was kept depressed for 500 ms post-stimulus, and released thereafter. RT was defined as the time when the monkey released the lever. GO and NO-GO trials were presented with equal probability in each session. The approximate electrode placements as marked visually during surgery are shown on schematic drawings of the lateral view of three macaque brains (Figure 3-1). The locations of all the electrodes were designated by arbitrary letters.

3.2.2 Data Analysis

In the present study, due to two reasons, the prestimulus time window was defined as (-90 ms, 35 ms). First, previous work (Ledberg et al., 2007) showed that the earliest evoked sensory responses occurred about 50 ms. This fact suggests 35 ms poststimulus activity doesn't interfere with the evoked activity. Second, the interval of the defined prestimulus period is 125 ms, including the lowest (8 Hz) frequency of alpha (8–14 Hz) oscillations.

Three LFP data sets, each including several sessions, were selected from three monkeys (TI, LU, and GE). Even in the same monkey, RT showed sizeable differences on the order of 150 ms or more. Since this study investigated the relationships between RT and prestimulus neural oscillations, only trials with correct GO responses were used. We preprocessed the LFP data by the following procedure. First, for each monkey, the trials having random responses (< 200 ms) or delayed responses (> 450 ms) were removed. Second, due to an insufficient number of trials of a single session for subsequent spectral analysis, it was essential to combine trials across sessions in each monkey. Third, to reduce session-to-session variability in each monkey, sessions having the similar statistical characteristics, including consistent averaged ERP waveforms, spectral power, and RT distribution, were selected. After rejecting outliers, bad channels and

sessions, three sessions in TI, five in LU, and three in GE respectively were used for subsequent analysis. Totally, 1000-1500 trials for each monkey were used in this study.

After preprocessing, trials were sorted by RT into 100-trial groups, starting with the fastest RT and proceeding to the slowest. To yield more groups, each group overlapped 50 trials with the previous one. Twenty one, twenty seven and eighteen groups for TI, LU, and GE respectively resulted. The RTs within each group were averaged to yield group mean RT.

Adaptive multivariate autoregressive power spectral analysis (Ding et al., 2000) was performed on each subensemble group during the prestimulus period. The subensemble mean at each site during the prestimulus period was subtracted from the individual prestimulus time series on each trial to ensure that the time series could be treated as coming from a zero-mean stochastic process, which is essential for the autoregressive spectral analysis. A model order of 8 was chosen by locating the minimum of the Akaike Information Criterion (AIC) (Akaike, 1974).

For each recording site, the Spearman-rank correlation coefficients (ρ) were computed between the power at each integer frequency in the range of 8- to 40-Hz and group mean RT. Thus, a multiple comparison correction was performed (14 sites and 33 frequencies in each monkey) by a permutation procedure (Nichols and Holmes, 2002). The order of group mean RT was randomly permutated for 500 times. At each permutation step, a maximum value of correlations over 14 recording sites and 33 frequency points was saved. All these maximum values were used to create a null-hypothesis distribution. By comparing the original correlation value to this permutation distribution we made sure that the probability for one correlation of having a significant effect at one frequency point occurring by chance was significant at $p <$ 0.05.

3.3 Results

The relationship between prestimulus spectral power (8–40 Hz) and group mean RT was examined here. The goal was to determine whether prestimulus spectral power was significantly correlated with RT, and if so, at which locations and which frequencies and this occurred. The correlations coefficients between spectral power and RT were found to significantly positive or negative, sometimes even non-significant, which depend on recording site and frequency. Figure 3-2 shows two examples from monkey TI. The power spectra from a prefrontal site (M) have a prominent peak at 16 Hz, whereas those from a striate site (B) don't show peaks at any frequency. On the bottom row, the scatter plots between group power at 16 Hz and group mean RT show a significant negative correlation (Spearman, $\rho = -0.91$, $p < 0.0001$) at site M and a significant positive correlation (Spearman, $\rho = .73$, $p < 0.001$) at site B. Here the p-values were calculated on a single recording site and single integer frequency basis.

Figure 3-3, 3-4, and 3-5 show the summarized results of the correlation analysis for all frequencies and sites in monkeys TI, LU, and GE, respectively. The horizontal axis displays frequencies from 8 to 40 Hz, and the vertical displays Spearman's rank correlation coefficients from -1 to 1. Gray shaded regions indicate the frequencies having spectral power that was correlated with group mean RT at $p < 0.05$.

Four main results were found. First, beta-band spectral power in the prefrontal cortex was negatively correlated with group mean RT in monkeys TI and GE. In monkey TI, of the four prefrontal sites (L, M, N, and O), three sites (L, M, and O) had significant negative correlation coefficients ($\rho < -0.70$, $p < 0.05$) in the frequency ranges 16–25 Hz, 12–24 Hz, and 17–32 Hz, respectively. In the other prefrontal site (N), the correlations in the frequency range 16–30 Hz were also negative, although these correlations did not reach statistical significance. In monkey GE, site O among the two prefrontal sites (N and O) also had significant negative correlations (ρ

29

< -0.62, p < 0.05) in the frequency range of 15–18 Hz. Only one prefrontal site (N) was recorded

from monkey LU and had insignificant correlations with group mean RT.

The second findings concern sites in the sensorimotor cortical areas from all three

monkeys. In LU, two (K and L) of three sites had significant positive correlations (ρ > 0.61, p <

0.05) over a broad frequency range from 8 to 33 Hz. The remaining site (M) had also positive

correlations in the frequency range of 8–22 Hz although they did not reach significance. In GE,

two (J and K) of four sensorimotor sites showed significant positive correlations (ρ > 0.62, p <

0.05) in the frequency range of 8–30 Hz. Power at the two sensorimotor sites (J and K) in TI was

not significantly correlated with group mean RT in the range of 8–40 Hz.

Third, the correlations found in the visual cortex were consistent across all three

monkeys. Here the visual cortical areas include striate, prestriate, and inferior-temporal recording

sites. Figure 3-3 shows that spectral power at all six visual cortical recording sites (B, C, D, E, F,

and G) in monkey TI had significant positive correlations (ρ > 0.65, p < 0.05) with group mean

RT, mostly in the range of 8–20 Hz. In LU, three (A, B, and D) of the six visual cortical sites had

significant positive correlations (ρ >0.61, p <0.05), primarily in the range of 8–18 Hz, whereas

the positive correlations found in the remaining three visual sites (C, E, and F) didn't reach

statistical significance. In GE, power at three (B, E, and F) of six visual cortical sites (A, B, C, D,

E, and F) had significant positive correlations (ρ > 0.65, p < 0.05) with group mean RT, and this

was mostly in the frequency band of 8–18 Hz.

Fourth, the superior-temporal recording sites in two monkeys (TI and LU) had positive

correlations with group mean RT. In TI, one superior-temporal site (H) showed significant

positive correlation (ρ > 0.73, p < 0.05) at 25–27 Hz. In LU, one of the two superior-temporal

sites (H) had significant positive correlations (ρ > 0.62, p < 0.05) in the range of 12–16 Hz. The

other site (G) had also positive correlations in the range of 8–25 Hz, which didn't reach significance. Monkey GE had no superior-temporal sites.

3.4 Discussion

In this study, we investigated the statistical relationship between prestimulus spectral power in the range of 8–40 Hz and RT over broad cortical regions. Our findings showed that prestimulus oscillatory activity was either positively or negatively correlated with RT in different cortical regions, which would indicate different underlying neural functions. Our main findings are summarized as follows: (1) spectral power in the prefrontal cortical sites, in the beta range (14–30 Hz), showed significant negative correlations with RT in two monkeys; (2) power at the visual cortical sites, in the alpha/low beta (8–20 Hz) ranges, was significantly positively correlated with RT in two monkeys; (3) power in the sensorimotor cortical sites, in alpha and beta ranges (8–30 Hz), showed significant positive correlations with RT in two monkeys.

The prefrontal cortex is highly interconnected with all cortical sensory and motor systems, and is believed to be situated at the highest level of the cortical executive hierarchy that controls attention, movement execution, and other cognitive functions (Brunia, 1999; Knight et al., 1999; Engel et al., 2001; Fuster, 2001; Miller and Cohen, 2001). In our study, the observed negative correlations of prestimulus neural oscillations in prefrontal cortex are consistent with a hypothesized role of the prefrontal cortex in mediating top-down control in anticipatory attention by sending modulatory 'bias signals' to lower-order sensorimotor circuits and thus enhance subsequent stimulus processing.. Liang et al. (2002) found that prestimulus beta oscillations in the prefrontal sites in one monkey TI was synchronized in a prefrontal network and was negatively correlated with RT. In a human EEG study, Silberstein et al. (2004) found that the increased phase synchronization over frontal recording electrodes prior to stimulus onset was correlated with faster RT, these results similar to our findings for these prefrontal sites. All the

findings suggest that before stimulus presentation the more enhanced attentional processing is mediated by the prefrontal cortex the faster is the behavioral response.

LFP activity within alpha and lower beta frequency band has been widely observed in the visual cortical areas of cats and monkeys (Eckhorn et al., 1988; Gray and Singer, 1989). Different hypotheses have been proposed to account for the role of these synchronized neural oscillations: cortical idling (Pfurtscheller et al., 1996b), inhibitory control and timing of cortical processing (Klimesch et al., 2007), and visual attentional disengagement (Foxe et al., 1998). Pfurtscheller *et al.* (1996) hypothesized that neural oscillations in the range of 8–20 Hz are characteristic of cortical areas that pass into an 'idling' state, in which no sensory and motor information is received or processed. Furthermore, Klimesch et al. (2007) proposed that alpha oscillations may reflect the inhibition control of conflicting or unnecessary sensory cortical processes to the tasks in hand by increasing signal to noise ratios within cortex. Foxe *et al.* (1998) reported that elevated alpha activity during the prestimulus time period at parieto-occipital regions indicated visual attentional disengagement during selective auditory attention when subjects were cued to the auditory rather than to the visual modality. These three hypotheses are not exclusive, and all of them agree with the idea that alpha and lower beta activity is inversely related to cognitive information processing. Our findings that alpha and lower beta activity at visual cortical sites was positively correlated with RT imply that higher levels of alpha and lower beta activity reflect lower levels of visual processing, hence leading to longer RT, which is concordant with the aforementioned hypotheses.

Oscillatory LFPs within the frequency range of 15–40 Hz have frequently been observed in the sensory and motor cortical circuit of nonhuman primates (Murthy and Fetz, 1992; Sanes and Donoghue, 1993; Baker et al., 1999). However, the functions of these oscillations are still

elusive. Some authors have proposed that these high-frequency LFP oscillations may play an active role for cortical binding between different motor areas and different parts of the motor system (Donoghue et al., 1998; Baker et al., 1999). Brovelli *et al* (2004) reported that a large-scale sensorimotor cortical network including the primary somatosensory cortex and primary motor cortex was bound together by prestimulus beta oscillations in supporting prestimulus motor maintenance of a fixed hand position. Our observation of positive correlations with RT in sensorimotor cortical sites further supports the hypothesized role of these oscillations in supporting motor maintenance behavior. That hypothesis is also line with the neural competition theory that a greater allocation of neural resources to the maintenance of hand position would be associated with larger high-frequency sensorimotor oscillations, and consequently longer RT to the visual stimulus would result.

In summary, we found that the spectral power of prestimulus oscillatory activities was correlated with response time in the range of 8–40 Hz, in prefrontal, sensorimotor, temporal, and visual cortical areas. Our findings suggest the positive or negative correlation is a useful index for sensory and motor processing over broad cortical areas. Hence, this approach investigating the relationship between ongoing activity and behavioral responses would enable us to tease out the functional role of these ongoing oscillatory activities.
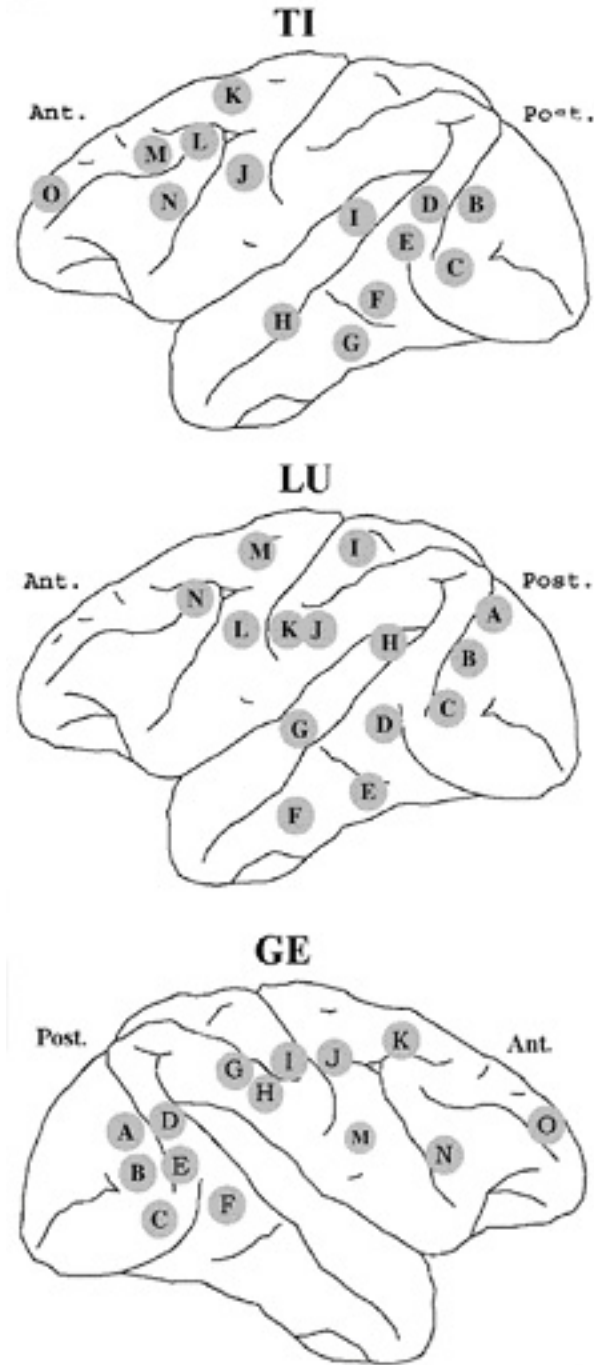
Figure3-1. Approximate electrode placements as marked visually during surgery in the three macaque monkeys, shown on schematic drawings of the lateral cortical hemispheres. The locations of all the electrodes are designated by arbitrary uppercase letters. The 'Ant.' indicates the anterior part of the hemisphere and the 'Post.' means the posterior part.
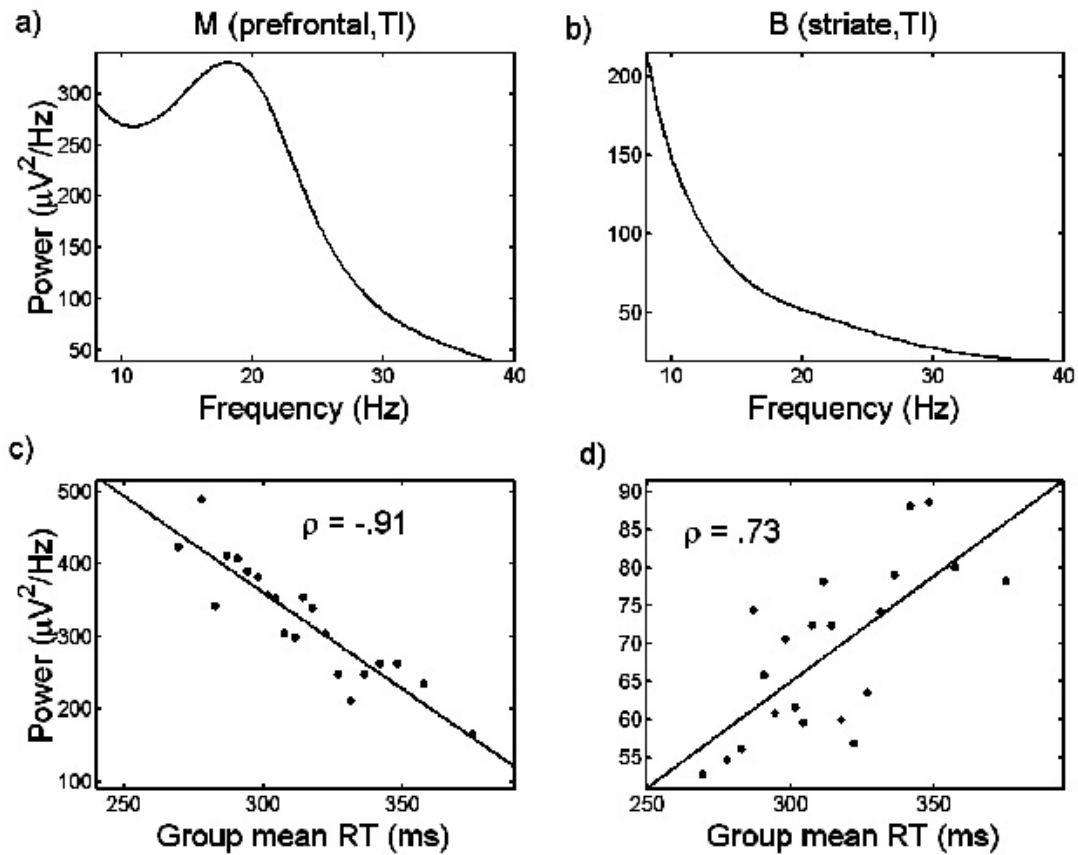
Figure 3-2. Prestimulus power spectra (8–40 Hz) and correlation plots for two recording sites in monkey TI. Top row: prestimulus power spectra for a prefrontal site (M) and a striate site (B). Bottom row: scatter plots showing significantly positive or negative correlations between prestimulus group spectral power and group mean RT at 16 Hz. The solid lines shown in c) and d) are superimposed linear least-square fits.
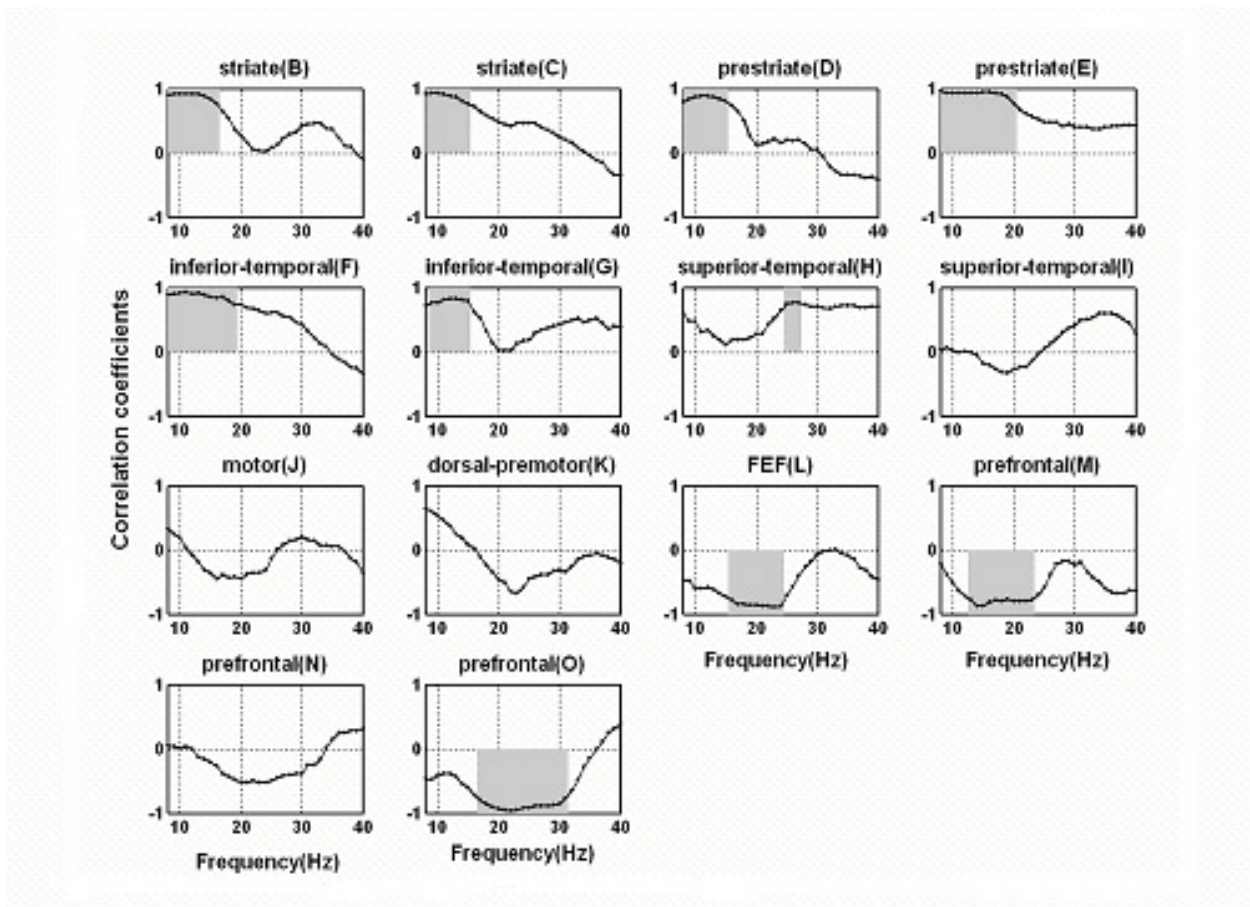
Figure 3-3. Spearman's rank correlation coefficients between prestimulus group spectral power and group mean RT for monkey TI. The horizontal axis indicates frequency in the range of 8 to 40 Hz. The vertical axis displays the correlations from -1 to 1. Gray shaded areas signify correlations that are significant at $p < 0.05$.
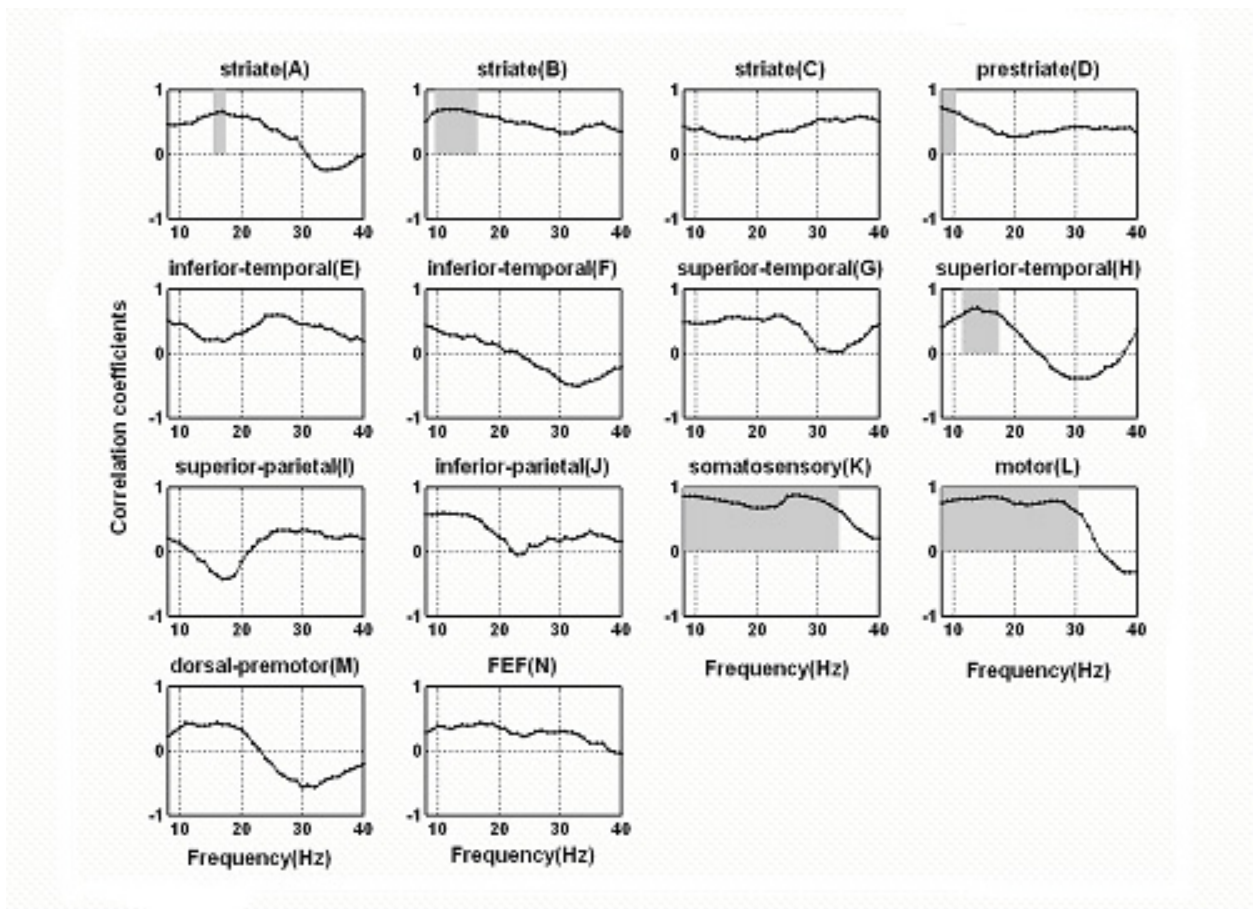
Figure 3-4. Spearman's rank correlation coefficients between prestimulus group spectral power and group mean RT for monkey LU. The horizontal axis indicates frequency in the range of 8 to 40 Hz. The vertical axis displays the correlations from -1 to 1. Gray shaded area signifies correlations that are significant at $p < 0.05$.
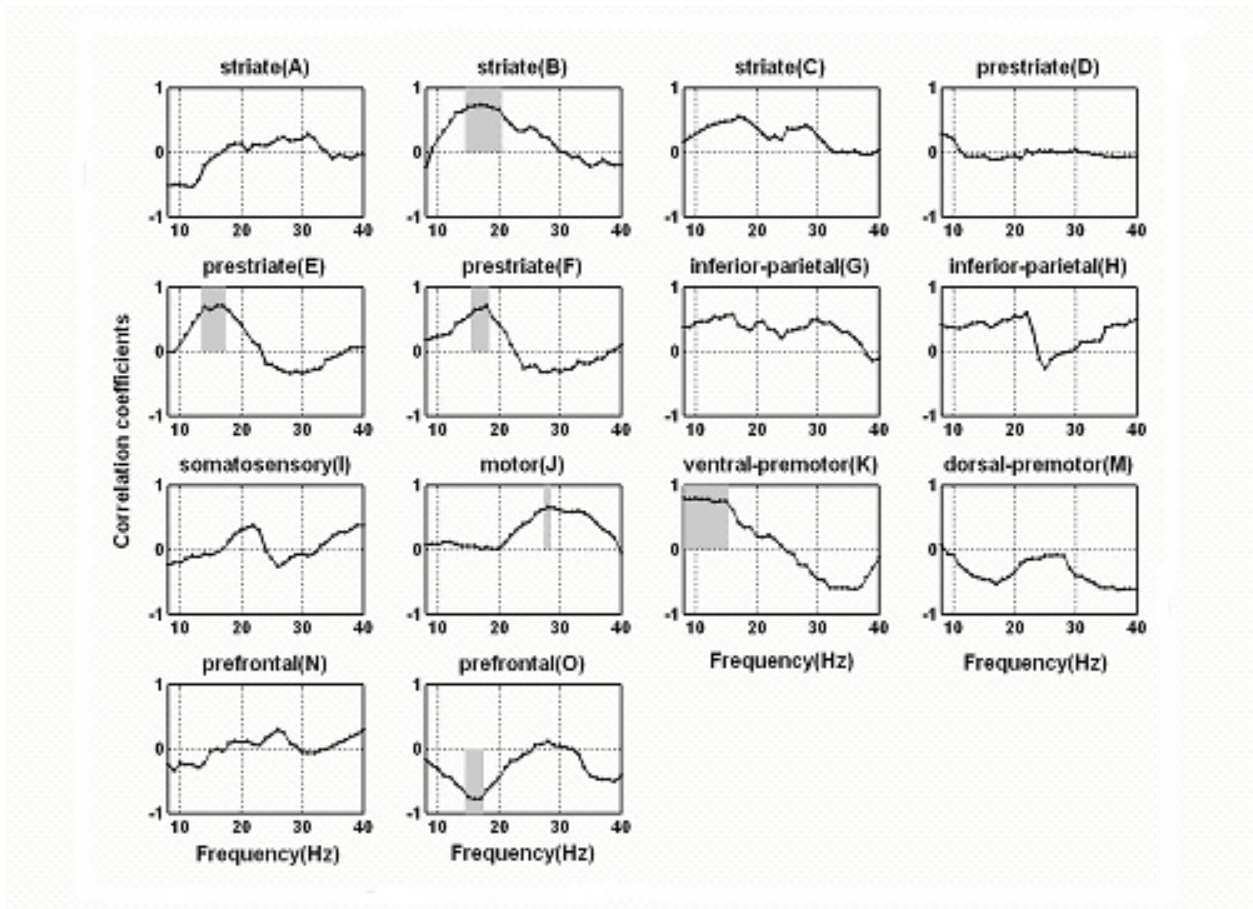
Figure 3-5. Spearman's rank correlation coefficients between prestimulus group spectral power and group mean RT for monkey GE. The horizontal axis indicates frequency in the range of 8 to 40 Hz. The vertical axis displays the correlations from -1 to 1. Gray shaded area signifies correlations that are significant at $p < 0.05$.

CHAPTER 4
CORTICAL SENSORIMOTOR RHYTHMS AND THEIR FUNCTIONAL ROLES

4.1 Introduction

Cortical sensorimotor rhythms, occurring in pre- and post-central cortical areas, usually include two frequency bands: 8–14 Hz and 15–30 Hz. These oscillatory neural activities have been widely observed in rodents, primates, and humans (Murthy and Fetz, 1992; Sanes and Donoghue, 1993; MacKay and Mendonca, 1995; Baker et al., 1997; Baker et al., 1999; Wiest and Nicolelis, 2003). A human MEG study (Salmelin and Hari, 1994) demonstrated that the lower frequency band (8–14 Hz) oscillations, called the mu rhythm, were most likely dominant in posterior somatosensory cortical areas whereas the higher frequency band (15–30 Hz) oscillations, called the beta rhythm, were originated in frontal motor cortical areas.

These neural oscillatory activities have been found to be synchronized between pre- and postcentral cortical sites (Murthy and Fetz, 1992; 1996), and between sensorimotor activity and muscle activity EMG (Conway et al., 1995; Halliday et al., 1998; Gross et al., 2000; Mima et al., 2000; Kilner et al., 2003). However, the functional significance of these synchronous neural oscillations in sensorimotor cortex is enigmatic.

It is well known that mu or beta oscillations occur before stimulus presentation and voluntary movement and suppress during movement execution. In a visuomotor GO/NO-GO task, the sensorimotor neural oscillations decrease markedly shortly after stimulus onset and rebound after a brief suppression in the NO-GO trials (Kuhn et al., 2004). In the Nakamura dataset described in Chapter 3, a strong beta rhythmic component was observed in the pre- and post-central cortical sites prior to stimulus presentation. A previous study (Brovelli et al., 2004) has characterized the prestimulus state of the motor system by applying power, coherence and Granger causality spectral analysis to local field potentials in a visuomotor discrimination task.

These authors showed that the pre-and post-central cortical sites was bounded by prestimulus beta oscillations and posterior somatosensory cortical sites exert causal influences on frontal motor cortical sites. Thus, due to consistent motor behavior in pre- and post-stimulus periods, the first goal of the present study was to test the hypothesis that the poststimulus rebounded neural beta oscillatory network has the same cortical dynamical organization as the prestimulus state. This was accomplished by characterizing the rebounded beta network with the same coherence and Granger causality analysis employed by Brovelli et al. (2004).

To explore the robustness of the first hypothesis and its feasibility on other measurement, the second goal is to test the hypothesis that during prestimulus time intervals the similar sensorimotor dynamical organization occurs in the similar scalp EEG experiment. Thus, we conducted the same visual pattern discrimination task, performed by normal human subjects. Adaptive multivariate autoregressive modeling techniques were applied to the prestimulus state to extract temporal functions of spectral power, coherence and Granger causality (Kaminski et al., 2001; Brovelli et al., 2004).

4.2 Methods and Materials

4.2.1 LFP Experiment and Data Preprocessing

Recording sites located in pre- and post-central cortical areas of two monkeys (4 in LU and 6 in GE) were selected for subsequent data analysis. A schematic of approximate electrode placement is shown in Figure 4-1. Trials having incorrect behavioral responses and artifacts were excluded. For each monkey, the experimental sessions having similar RT histograms were combined to yield approximately 1000 GO trials and the matching numbers of NO-GO trials were selected from the same sessions.

Time-frequency power spectral analysis was applied to determine the beta rebound onset in the NO-GO condition. Each sliding window was 100 ms in length and slid 5 ms forward. A

total of 101 windows was resulted for the entire trial time period (-90 ms, 505 ms). Power in the 15–25 Hz range averaged over all pre- and post-central sites was plotted as a function of time (Figure 4–2). The following procedures were used to detect the onset latency of beta rebound: identify the minimum value of post-stimulus beta power and determine the time (defined as the onset latency of beta rebound) at which this beta power increased by at least 10% above this minimum.

Adaptive MultiVariate AutoRegressive modeling method (Ding et al., 2000; Ding et al., 2006) was applied to the poststimulus window. To treat the residuals as coming from a zero-mean stochastic process which is essential for AMVAR data modeling (Ding et al., 2000), the ensemble mean was removed from each trial for each recording site. A model order of 10 was determined by the Akaike Information Criterion (Akaike, 1974).

Spectral power, coherence, and Granger causality was calculated in each analysis window. Spectral power reflects the degree of neural synchronization in a local neural ensemble. Coherence estimates the degree of neural synchrony between two distant neural ensembles. Granger causality further gauges whether one neural ensemble exerts a causal influence on another. Significance testing for coherence and Granger causality was accomplished by a random permutation procedure (Nichols and Holmes, 2002). Details have been described in Brovelli et al. (2004).

In Brovelli et al. (2004), the time interval (-90 ms, 20 ms) was defined as the wait window for both GE and LU. In the present study, to investigate the dynamical organization of the rebound beta sensorimotor network after its brief suppression in the NO-GO condition, based on the onset latency of beta rebound in each monkey, a post-rebound window was selected and referred to as the recurrence window, (395 ms, 505 ms) for GE and (300 ms, 505 ms) for LU.

Coherence and Granger causality analysis was performed for the recurrence window and compared with the known results obtained from the same data sets during the prestimulus time period (Brovelli et al., 2004).

4.2.2 EEG Recording and Paradigm

We applied the same AMVAR modeling analyses to scalp EEG recordings and investigated characteristics of the sensorimotor dynamical organization in two conditions: hold and rest. Human participants (3 males, average 28 years old) were trained to perform the same visual-motor pattern discrimination task in an acoustically and electrically shielded EEG booth. The study was approved by the Institutional Review Board of University of Florida.

At the beginning of experiment, baseline eye-closed rest EEG signals were recorded for 5 min. Before stimulus presentation, participants were given a visual cue to press and hold steadily a response key on a response panel with the right index finger for at least 800 ms. In the hold condition, the prestimulus time interval was defined as (-300 ms, -10 ms). In the rest condition, the continuous baseline EEG data were epoched to the matching number of trials and the matching length of each trial. Granger causality spectral analysis was applied to measure directional influences among the appropriate EEG electrodes representing primary somatosensory, frontal motor, and posterior parietal areas. According to the international 10-10 system, the EEG electrodes contralateral or ipsilateral to the performing hand about 2 cm posterior to C3/C4 were used for left or right S1 activity (LS1 or RS1), electrodes at FC3/FC4 were selected to reflect activity of the frontal motor areas, and the site at Pz was chosen to represent the posterior parietal activity.

4.3 Results

4.3.1 LFP Results

For each monkey, power spectra were computed for each of the sliding analysis windows and averaged across all recording sites over the entire trial time period. Figure 4-2 shows the power result for GE (A, left column) and LU (B, right column) where the GO condition is in the top row, the NO-GO condition in the middle row, and the bottom row is the averaged beta band power as a function of time. In the NO-GO condition, beta activity rebounded significantly at approximately 300 ms for GE and approximately 260 ms for LU. The rebounded beta activity was sustained until the end of the trial. Note that the rebounded beta oscillations in LU were stronger than that existing prior to stimulus presentation whereas those in GE were weaker compared with the prestimulus state.

Coherence spectra for all site pairs and Granger causality spectra in both directions for all site pairs were computed over the recurrence window. Figure 4-3 shows that the beta activity in power, coherence, and Granger causality spectra was prevalent in the recurrence window. Three recording sites common to both monkeys were selected: primary somatosensory (S1), primary motor (M1) and inferior posterior parietal area 7b. The coherence and Granger causality spectra were averaged in the beta frequency range. The threshold for significant coherence at $p < 0.005$ was determined to be 0.020 for GE and 0.016 for LU, and that for significant Granger causality was 0.012 for GE and 0.011 for LU.

In the wait window, the previous study (Brovelli et al., 2004) showed that the anterior postcentral (primary somatosensory cortex) sites (S1) played a clear role as a driver to precentral (motor cortex) site (M1) and to post-central (inferior posterior parietal cortex) sites (7b), with the latter one exerted causal direction to motor cortex. In the recurrence window, these main causal influences (S1-M1, S1-7b, and 7b-M1) were similar to those in the wait window, except that

motor cortex also sent feedback causal influences back to 7b in LU. Figure 4-4 shows that both monkeys GE and LU had the similar dynamical organization in the recurrence window to those in the wait window. Only significant Granger causality values greater than the threshold were shown.

Our findings from the Nakamura dataset were that the large-scale sensorimotor cortical networks were bound by beta oscillations during wait window and recurrence window and dissolved during movement execution. In both premovement and poststimulus hold periods, Granger causal influences were carried from S1 to both M1 and 7b, and 7b also exerted Granger causal influences on M1, in agreement with the idea that somatosensory feedback is essential for the sensorimotor system to maintain a constant motor output.

4.3.2 Scalp EEG Results

Figure 4-5 shows the Granger causality spectra from the left S1 electrode (LS1) to the left frontal motor electrode (FC3) for the prestimulus period condition and the baseline EEG condition. The directional influences in the range of 8–20 Hz, peaking at 11 Hz, were largely enhanced for the hold condition whereas those in higher (20–40 Hz) frequency range are not different between the two conditions. The pairwise directional influences from five electrodes were summarized in Figures 4–6 A and 4–6 B. The lines connecting different cortical areas correspond to averaged Granger causality values between 8–14 Hz and only the values greater than 0.05 were shown. The arrowheads indicate the direction of Granger causal influence.

For the hold condition, the cortical areas in the left hemisphere are more actively interacted than those in the right hemisphere. The left S1 cortical area drives left frontal motor cortical areas and bidirectionally interact with right frontal motor and posterior parietal cortical areas, whereas the right S1 cortical areas do not receive or exert any causal influences. For the baseline condition, the main driver is posterior parietal cortex and left or right S1 cortical areas

are not engaged in any sensorimotor networks. All the results are in line with the functional role of the primary somatosensory cortex in the maintenance of a steady motor output. Hence, the main sensorimotor dynamical organization in humans and nonhuman primates performing the same tasks are remarkably consistent.

4.4 Discussion

For voluntary movement, the post-movement mu or beta rebound is thought to reflect an idling state of the brain (Pfurtscheller et al., 1997a) or active immobilization (Salmelin et al., 1995), and is thought to be independent of sensory input (Salmelin et al., 1995; Pfurtscheller et al., 1996a). In the present study, the mu or beta oscillations took place in the conditions when there was no overt movement, prestimulus hold periods and poststimulus rebound periods.

Our previous work analysis for the prestimulus periods found that beta activity mediated the causal influences from primary somatosensory cortex (S1) to posterior parietal area 7b, and from both S1 and 7b to primary motor cortex M1 (Brovelli et al., 2004; Chen et al., 2006). Based on these previous results, it was hypothesized that the functional role of the sensorimotor beta network is to facilitate the sensorimotor integration of sensory feedback information for the maintenance of the depressed hand lever. As the lever pressure was maintained, it is thus reasonable to suggest that beta rebound signaled the resumption of the same network in support of sensorimotor integration.

Similarly, the same pattern of these dynamical organizations during hold period in EEG recording was also found, even though these sensorimotor networks are mostly active in mu not beta frequency range. Thus, no matter prestimulus or poststimulus hold periods, the functional connectivity plays a key role serving to maintain steady motor output.

Our network analysis results are thus in line with recent studies that postulate an important role for sensory feedback in coherent mu or beta oscillatory activity (Conway et al.,

1995; Baker et al., 1997; Baker et al., 1999; Mima et al., 1999; Kilner et al., 2000; Kilner et al., 2003; Brovelli et al., 2004; Houdayer et al., 2006). Baker et al. (1997, 1999) showed that, during a precision grip task, sensorimotor beta oscillations were coherent with contralateral hand EMG. Cassim et al. (2001) reported that beta synchronization disappeared after subjects were sensory-deafferented.

In summary, cortical sensorimotor rhythms (mu or beta) play a crucial role in binding a large-scale sensorimotor oscillatory network and thus facilitate sensory integration of sensory feedback information to the motor system, which is part of the cortical portion of a control loop serving to maintain steady motor output.

GE   LU
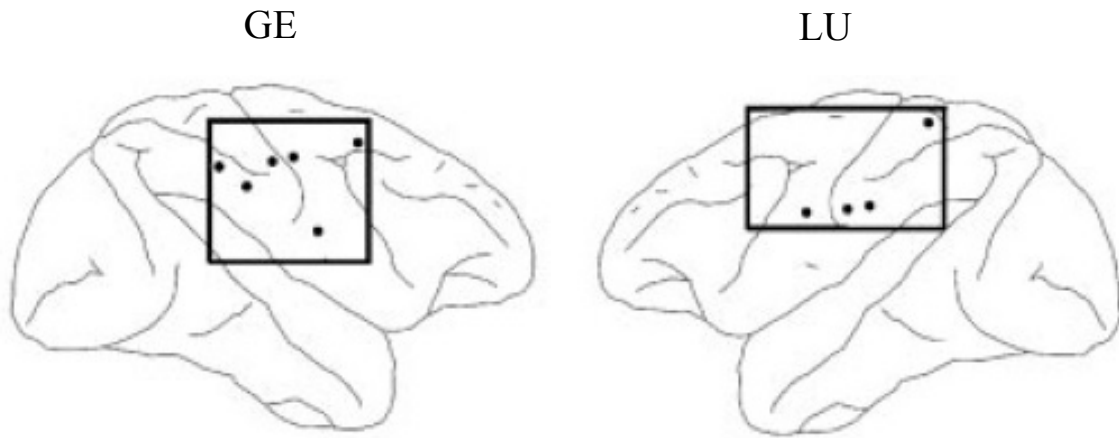
Figure 4-1. A schematic of approximate electrode placement in monkey GE (left hemisphere) and LU (right hemisphere). Black dots indicate electrode locations.
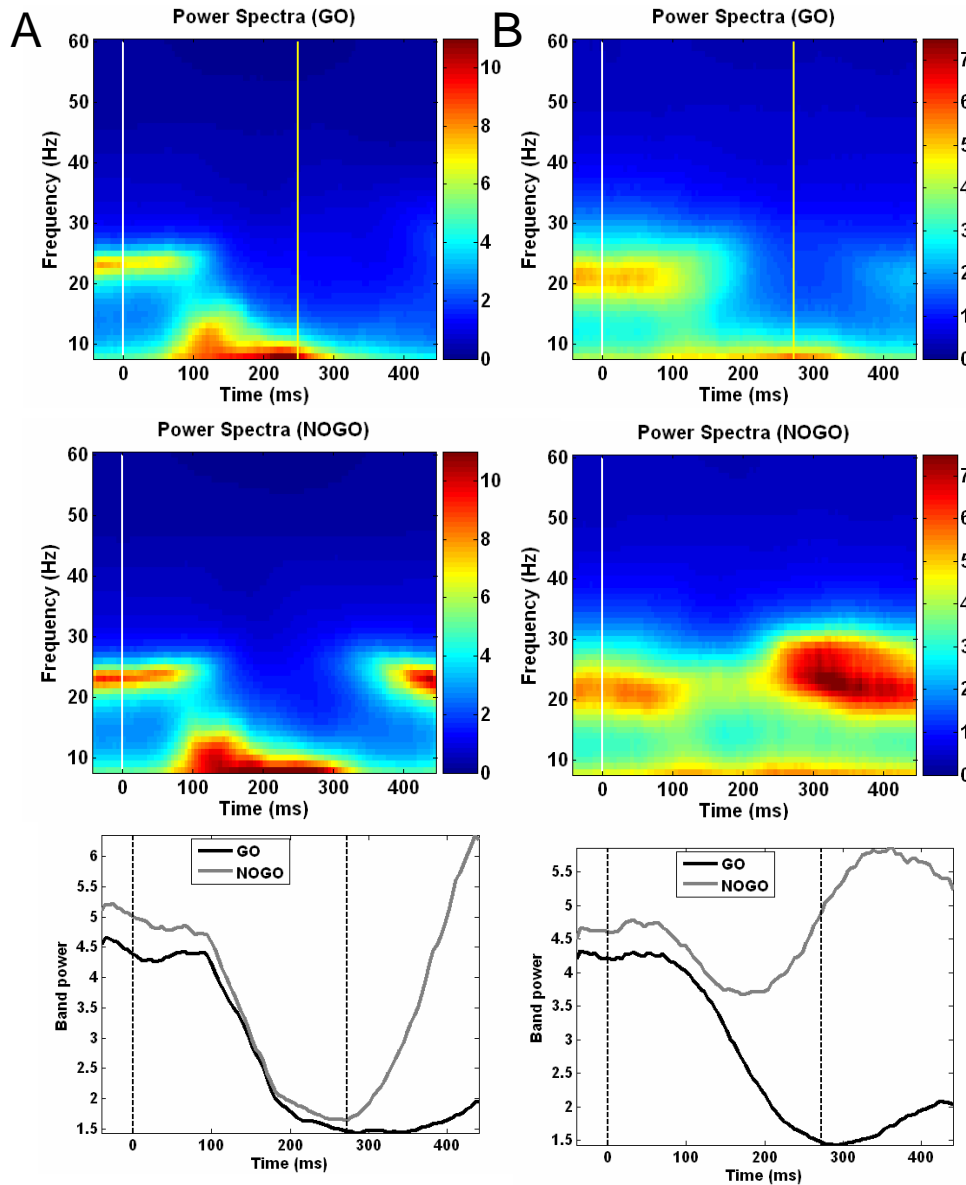
Figure 4-2. Time-frequency plots of averaged power spectra computed over all sites in GE (A) and LU (B). Average beta power as function of time for both GO and NO-GO conditions are shown in the bottom row. The color scale indicates the values of power spectra. The vertical lines shown in pictures were stimulus onset (0 ms) and average response time, respectively.
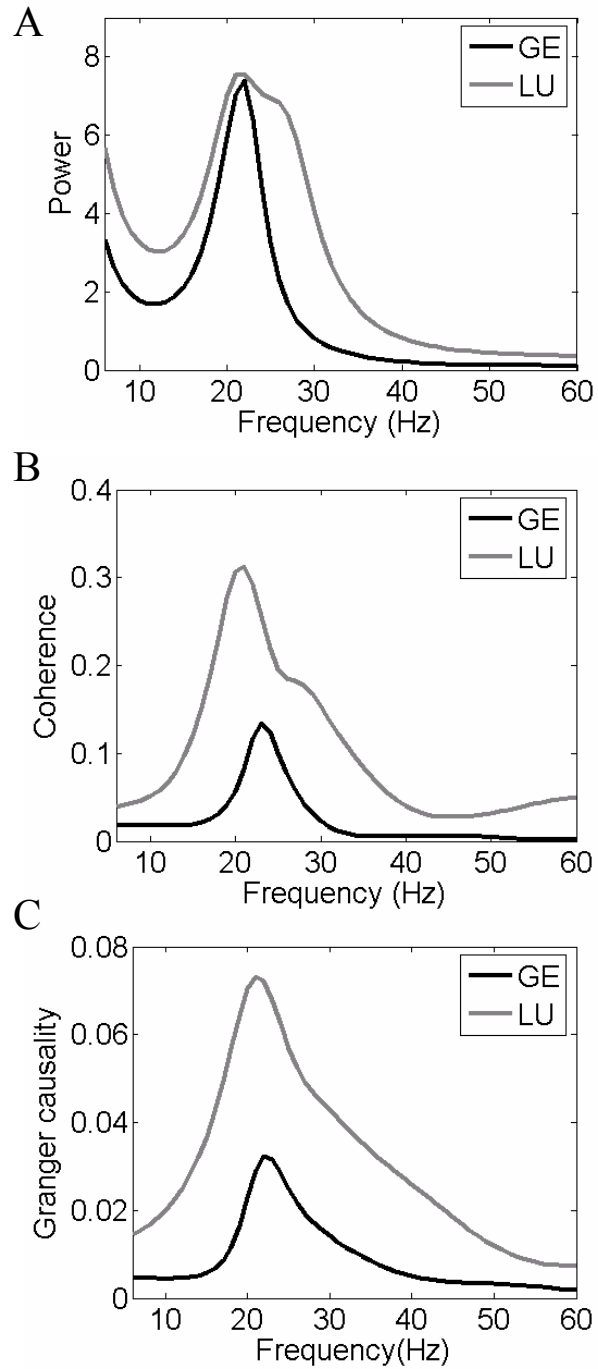
Figure 4-3. Averaged power spectra (5–60 Hz) over three selected sites (S1, M1, and 7b) (A), and averaged coherence spectra (B) and averaged Granger causality spectra (C) computed over all pairwise combinations in the recurrence windows for LU (gray curves) and GE (black curves), respectively.

GE

LU
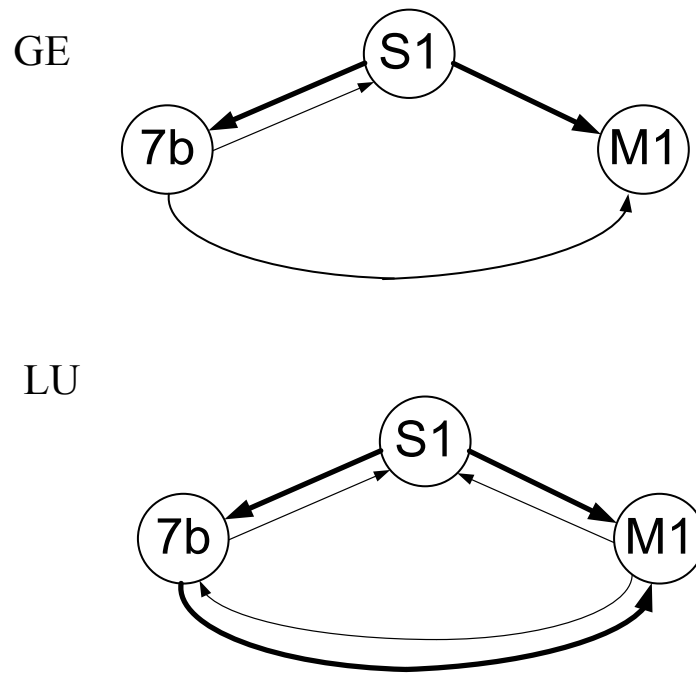
Figure 4-4. Schematic Granger causality graphs during the recurrence window in GE (top) and LU (bottom). The thickness of the lines between three recording sites and the numbers near the lines indicate the averaged Granger causality values in beta frequency range. The arrowheads indicate the direction of Granger causality influences. S1: primary somatosensory cortex, M1: primary motor cortex and 7b: posterior parietal cortex.
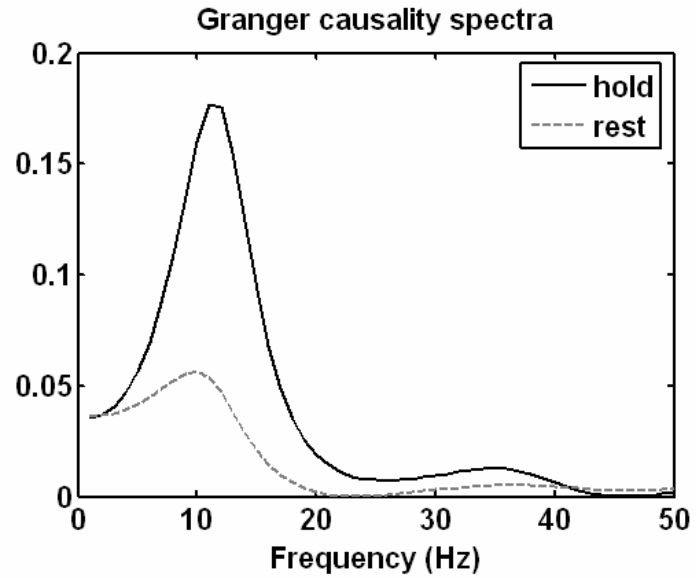
Figure 4-5. Granger causality spectra from left S1 cortical areas (LS1) to left motor cortical areas (FC3) for the prestimulus holding period (solid line) and the eye-close rest period (dashed line).
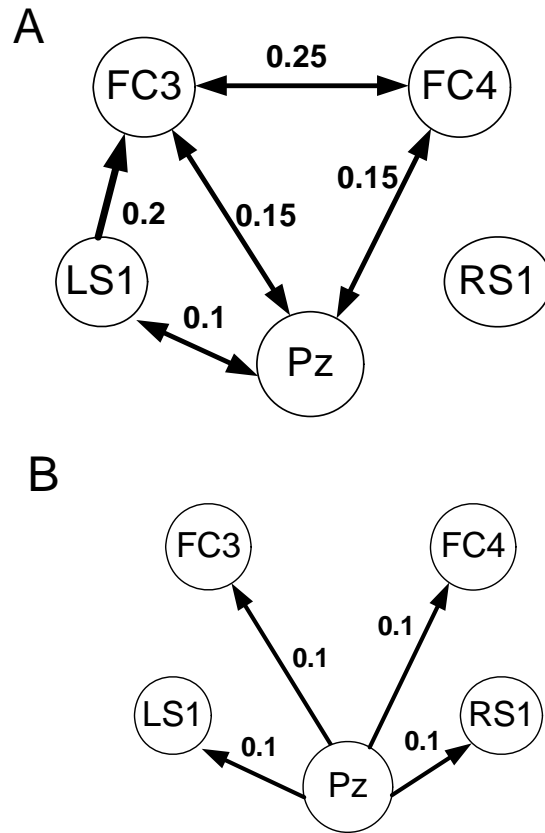
Figure 4-6. Granger causality Graphs for (A) the prestimulus time holding period and (B) the baseline condition. LS1 (RS1): left (right) primary somatosensory cortex.

CHAPTER 5
NEURAL CORRELATES OF SOMATOSENSORY PROCESSING OF A WEAK STIMULUS

5.1 Introduction

5.1.1 Somatosensory Evoked Potentials

Somatosensory evoked potentials (SEPs) are time-locked electrical signals in response to tactile, electrical and other somatosensory stimuli. Since scalp-recorded SEPs were first found by George Dawson in 1940s, analyses of SEP components have been widely used in clinical diagnosis of various brain, brainstem and spinal cord disorders, such as multiple sclerosis, spinal cord trauma, coma and peripheral nerve lesions (Kraft et al., 1998). In addition, SEPs are extensively studied in various cognitive tasks.

In human scalp EEG recording, SEPs (< 200 ms) have several components N20 (20–25 ms), P60 (50–70 ms), N80 (70–90 ms), P100 (90–110 ms), and N140 (110–160 ms) (P, positivity; N, negativity; numbers, msec from stimulus onset). The N20 component, reflecting the initial activation of peripheral somatosensory input in cortical areas, stems from area 3b of S1 (Allison et al., 1989) and varies solely as a function of stimulus intensity (Lesser et al., 1979). P60 (or P50) also originates in contralateral S1 (Allison et al., 1992) and mainly encodes the parameters of sensory stimuli even though it is slightly affected by cognitive factors (Desmedt and Tomberg, 1989; Tomberg and Desmedt, 1996). N80 is also recorded in contralateral S1 (Allison et al., 1989) and independent of sensory perception and attention (Schubert et al., 2006). The P100 component is generated from SII areas (Allison et al., 1992) and is sensitive to target stimuli (Desmedt and Robertson, 1977; Desmedt et al., 1983). Due to different experimental conditions and recording methods, the late SEP components (>200 ms), including N250 and P300, are also reported. In the present study, only the middle-latency somatosensory evoked potential—N140, highly correlated with somatosensory perception and attention, is discussed.

The somatosensory N140 component (110–160 ms, termed here N1 component), being

functionally analogous to the visual or auditory N1 component, is the large-amplitude slow SEP

component, appearing first in the contralateral S1 and S2 cortical areas and then in ipsilateral S1

and bilateral frontal areas. The amplitude of the N1 component is significantly affected by both

exogenous (e.g., stimulus intensity) (Nakajima and Imamura, 2000) and endogenous (e.g.,

attention) factors (Desmedt and Robertson, 1977; Allison et al., 1992; Garcia-Larrea et al., 1995;

Nakajima and Imamura, 2000; Giaquinto and Fraioli, 2003; Schubert et al., 2006). For example,

N1 amplitude is enhanced with increase in stimulus intensity and attention. N1 amplitude is

vulnerable to short ISI (< 400 ms) (Tomberg et al., 1989; Kekoni et al., 1997; Kida et al., 2004).

Additionally, the latency of the N1 component is hardly affected by the intensity of stimulus

(Nakajima and Imamura, 2000) and cognitive tasks (Desmedt and Robertson, 1977; Desmedt and

Tomberg, 1989).

5.1.2 Correlation of N1 and Sensory Attention

When a near-threshold somatosensory stimulus is presented, it may or may not be

perceived. Such perceptual outcomes are believed to be reflected by somatosensory evoked

responses. In a pioneer study, Libet and his co-workers (Libet et al., 1967) demonstrated that the

early somatosensory evoked responses, recorded subdurally in patients, had no significant

differences between conscious and unconscious experiences whereas the late responses was

deficient in unconscious experiences. A similar finding was reported in awake monkeys (Kulics

and Cauller, 1986; Cauller and Kulics, 1991) that the early surface-positive component (P1, 13

ms) was associated with multiple unit activity (MUA) in the middle layers and signaled an

earliest thalamocortical activation of S1 whereas the late surface-negative component (N1, 45

ms), a sensitive index of behavior performance, was associated with current sinks in superficial

layers I/II and elevated MUA in layers III-V.

Hence, based on the behavioral responses, human scalp N1 component, correlated with sensory attention, is functionally similar to those of the aforementioned surface-negative evoked responses. In a scalp EEG study, according to the scalp topography and behavioral performance, Garcia-Larrea et al. (1995) suggested that somatosensory N1 component could be split in two components: N120 (110-130 ms) and N140 (130-160 ms). The N120 component originates in contralateral S2, occurs in both neutral and attended conditions, and therefore is suggested to be associated with somatosensory awareness, whereas N140 component, observed only in attended conditions, occurs first in contralateral hemisphere and then is bilaterally distributed. Hence, N140 component is linked to spatial attention of stimuli and reflects activation and reciprocal interactions among several areas, such as, prefrontal cortex, supplementary motor cortex, and other subcortical structures (Allison et al., 1989; Desmedt and Tomberg, 1989; Allison et al., 1992). Here our current research mostly focuses on the attention effects of the N1 component.

It is known that attention causes stronger neural responses to weak stimuli than those to strong stimuli (Reynolds et al., 2000). When the effect of the exogenous factors on N1 component becomes smaller, the effect of endogenous factors on N1 becomes bigger. Hence, the neural basis of N1 component to a near-threshold stimulus, are explored in the present study.

5.1.3 Spontaneous Mu Rhythm

Mu rhythms (7–13 Hz), also called rolandic, wicket or center rhythms, gradually gain more and more attention since 1950s (Gastaut and Bert, 1954; Chatrian et al., 1959). The research on mu oscillations is carried out in many broad areas, including brain computer interface (Pineda et al., 2000), movement disorders (Oberman et al., 2005; Bernier et al., 2007), and smoking addiction (Pineda and Oberman, 2006). In some studies, mu rhythms sometimes also include sensorimotor signals in 15–25 Hz range, which are prevalent in pre-central gyrus

55

(Salmelin and Hari, 1994). In the present study, mu rhythms refer to the neural oscillations in the 7–13 Hz frequency range in the post-central gyrus.

Spontaneous mu rhythms have been observed in scalp EEG/MEG recordings from many healthy humans (Makeig et al., 2002). Figure 5-1 A shows the time traces of spontaneous mu rhythms during eye-closed rest. Mu rhythms have rhythmic waxing and waning patterns and the length of each mu segment is around 0.5-2 s.

Spontaneous mu oscillations were found to attenuate significantly by movement onset (Pfurtscheller et al., 1997b), movement observation and imagination (Pineda et al., 2000), and somatosensory stimulation (Salenius et al., 1997; Wiest and Nicolelis, 2003), and to increase during visual sensory processing (Pfurtscheller et al., 1996b). Therefore, these facts are taken as evidence that spontaneous mu oscillations reflect idling or deactivated somatosensory cortical areas (Kuhlman, 1978; Pfurtscheller et al., 1996b; Pfurtscheller et al., 1997b), which implies that spontaneous mu oscillations are uncorrelated with somatosensory processing.

Furthermore, according to the phenomenon that the neural synchronization in the alpha or alpha-like rhythms was observed in retention period and the desynchronization was associated with memory retrieval (Klimesch et al., 1999; Jensen et al., 2002), an inhibition-timing hypothesis (Klimesch et al., 1999; Klimesch et al., 2007) is proposed that the synchronization in alpha range blocks the retrieval of previous items, avoids the encoding of new items, and thus reflects the top-down inhibitory control over task-irrelevant brain areas. On the other hand, an alternative interpretation is that these neural activities are involved in coupling broad cortical areas and sustaining memorized items (Jensen et al., 2002; Palva and Palva, 2007).

5.1.4 N1 and Ongoing Activity

Past research has reported conflicting results concerning how N1 amplitude is associated with ongoing mu or alpha power. The positive (Brandt et al., 1991; Arieli et al., 1996; Nikouline

et al., 2000), negative (Rahn and Basar, 1993; Chen et al., 1999; Ploner et al., 2006), or non-significant (Simoes et al., 2004) correlations were found. These conflicting findings may be partly due to experimental conditions and methodological differences, such as, recording techniques, stimulus intensity, and ERP measurement.

Nevertheless, these conflicting findings also imply that the relationship between ongoing mu (or alpha) activity and N1 amplitude may be not monotonic. In a recent MEG study, Linkenkaer-Hansen et al. (2004) found that the intermediate level of prestimulus mu power immediately preceding a weak electrical stimulus was correlated with the highest probability of sensory detection, which suggested that prestimulus mu oscillations optimize stimulus processing through intrinsic stochastic resonance (Ho and Destexhe, 2000; Stocks and Mannella, 2001).

In addition, N1 amplitude is also significantly affected by the phase of spontaneous ongoing mu or alpha oscillations before stimulus presentation. Jansen and Brandt (1991) demonstrated that the trials having the phase of positive-going zero crossing at stimulus onset had maximal N1 amplitudes, whereas the trials having negative-going zero crossing has minimal N1 amplitudes. Since the latency of N1 component is in the alpha frequency range and N1 amplitude is affected by prestimulus alpha power, they thought N1 component might be a part of entrained alpha activity. Furthermore, Makeig and his coworkers proposed the phase-resetting hypothesis (Makeig et al., 2002), which suggested that ERPs are partly generated by the phase-resetting of multiple ongoing EEG processes. In the present study, we only considered the effect of prestimulus mu power on N1 and thus the random distributions of ISI were used here.

Hence, given the preponderance of evidence linking higher N1 amplitude with increased sensory processing, we predict that an inverted-U relationship also exists between prestimulus

mu oscillations and N1 amplitude. It means that the intermediate level of prestimulus mu power prior to stimulus onset facilitates cortical sensory processing whereas too much or too little mu power may reduce the efficiency of perception.

5.1.5 N1 and Top-down Attentional Control

Cauller and Kulics (1986, 1991) postulated that somatosensory N1 component was generated by the interaction between feedforward projections from ascending signals and feedback projections from other higher order cortices, including S2, frontal, and posterior parietal cortical areas (Cauller and Kulics, 1991; Cauller, 1995; Cauller et al., 1998; Jackson and Cauller, 1998; Staines et al., 2002; Golmayo et al., 2003). In other sensory modalities, the similar results that the re-entrant processing is essential for sensory perception were found (Lamme and Roelfsema, 2000). These feedforward and feedback projections are believed to be implemented by neural oscillations (Engel et al., 2001; Buschman and Miller, 2007).

An increasing number of studies suggested that alpha or alpha-like rhythms were sensitive to various cognitive and attentional tasks and likely played significant roles in stimulus sensory processing (Halgren et al., 2002; Jensen et al., 2002; Serrien et al., 2004; Pineda, 2005; Pollok et al., 2005; Sauseng et al., 2005a; Sauseng et al., 2005b; Klimesch et al., 2007; Palva and Palva, 2007). Sauseng et al. (2005) reported that the increased prefrontal alpha synchronization was associated with occipital alpha suppression in a working memory task and prefrontal alpha oscillations modulated occipital alpha oscillations by investigating alpha latency shifts. It supports previous studies that the corticocortical synchronization in the alpha frequency range may play a significant role in top-down processing (von Stein et al., 2000). Furthermore, the global binding hypothesis (Nunez et al., 2001; Pineda, 2005) was proposed that all the alpha-like rhythms, locally independent, become coupled and translate all sensory inputs into perception

and action. In addition, a recent simulation study (Vanrotterdam et al., 1982) showed that alpha oscillations were available for a large-scale cerebral integration.

Most of these aforementioned findings focus on the functional significance of neural synchronization during stimulus processing. However, ongoing neural activity prior to the presentation of stimulus, reflecting anticipation and prediction to forthcoming sensory and motor events, attracts increasing interest (Arieli et al., 1996; Kastner et al., 1999; Tsodyks et al., 1999; Engel et al., 2001; Dehaene and Changeux, 2005). It is suggested that the intrinsic bias signals from high-order cortical areas might create a facilitatory brain state conducive to sensory perception.

To achieve the better understanding the relationship between ongoing mu activity and subsequent somatosensory processing, we investigated 1) the relationship between ongoing mu oscillations and stimulus evoked N1 amplitude; 2) the functional role of top-down signals from prefrontal cortex and other frontal areas in sensory perception and in the modulation of N1 amplitude.

5.2 Materials and Methods

5.2.1 EEG Experiment and Design

A somatosensory perception EEG experiment was performed in an acoustically and electrically shielded booth. EEG signals were recorded from thirteen right-handed participants (24-38 years of age, 3 females), who were free of any movement disorders and neurological diseases. Participants were given informed consent before participation and were paid $30 for their participation. The study was approved by the Institutional Review Board of University of Florida.

Before the experiment, baseline EEG was recorded during eye-closed rest for 5 min. To avoid visual modulation of somatosensory processing (Taylor-Clarke et al., 2002) and minimize

eye blinks and eye movement, participants were asked to close their eyes during the experiment. Both hands of participants were resting on a table in front of them. A pair of stimulation electrodes, 2 cm apart, were placed on the distal (anode) and middle (cathode) phalanges of the right index finger. The left hand was resting on the ERTS response panel. A biphasic near-threshold electrical stimulus (0.3 ms duration) was delivered to the right index finger tip. Participants were asked to press a button by the left index finger as quickly as possible when they felt the electrical stimulus. The maximal intensity of electrical stimuli was less than 5 mA. Electrical stimulus onset was defined as 0 ms. The interstimulus intervals varied randomly between 4500 ms to 5000 ms in 6 steps. The intensity of the electrical stimulus was adjusted to each individual subject's threshold using a staircase method (Leek, 2001). At the threshold intensity the subject was able to perceive half the stimuli. The stimulus intensity is kept the same for the entire experiment. The experiment for each subject includes at least 10 blocks each having 40 stimulation trials. To minimize learning and adaptation effects, before the experiment started, participants were given 40–80 practice trials. A few breaks were given between blocks.

The EEG data were acquired by a 128-channel BioSemi ActiveTwo system (http://www.biosemi.com). Four extra electrodes placed around the eyes were used to record horizontal and vertical eye movement. Two electrodes were placed in the left and right mastoid. EEG signals were sampled at 2048 Hz online, down-sampled to 250 Hz offline, and bandpass filtered (0.3–50 Hz). EEG electrode locations were obtained by an electromagnetic 3 dimensional digitizer (Polhemus Corp). Electrical stimuli were delivered by a Grass stimulator (model S48). Response time was recorded by the EXKEY microprocessor logic of BeriSoft Experimental Run Time System (ERTS) system.

5.2.2 Data Preprocessing

Trials having incorrect responses (participants responded automatically without stimulus presentation) or contaminated by EOG or other artifacts (> 100 µV) were excluded from further analysis. In one or two specific subjects, second-order blind identification algorithm (Belouchrani et al., 1997) was applied to remove big EOG artifacts and outliers. The trials having response time occurring from 0.15 s to 2.5 s after stimulus onset were accepted for further analysis. Skin conducted stimulation artifacts occurred between -10 ms to 10 ms. Average reference was applied for subsequent analysis. Here we preferred not to apply Laplacian algorithms to remove common reference and volume conduction, due to underestimation of coherence and Granger causality by spatial filtering (Nunez et al., 1999). All data analysis was performed with BESA 5.0 (Brain Electrical Source Analysis, MEGIS software GmbH, Munich, Germany), SPSS (Statistical Package for the Social Sciences), MATLAB (Mathworks Inc.), and custom Matlab software.

SEP amplitudes were estimated with baseline-to-peak. Baseline correction was performed using the time interval (-100 ms, -20 ms). For each subject, the representation areas of the finger in contralateral S1 cortex was determined by the maximum positive deflection of the SEP components from 50 ms to 70 ms and also by scalp current density (SCD) maps (Perrin et al., 1987) (Figure 5-3 B). The SCD map, generated in BESA 5.0, is an estimate of the second spatial derivative of the voltage potential. It shows the scalp areas where the current either emerges or sinks between the scalp and the brain. Several EEG electrodes were selected to represent activities in cortical regions of interest (ROI). The SCD map at 60 ms shows the two EEG electrodes (usually 2 cm posterior to C3) are included in the approximately same current contour. Therefore, in the present study, these two electrodes were selected to represent contralateral S1 recording sites. Three electrodes (Fpz, Fp1, and Fp2), according to the International 10-10

System, were selected to represent prefrontal sites (Homan et al., 1987). An electrode (Oz) was selected to represent an occipital cortical site. The other electrode (Pz) was selected to represent a posterior parietal cortical site. Statistical significance level was defined as $p < 0.05$.

5.2.3 Correlation of Prestimulus Mu Power and N1

For each individual, prestimulus mu power of a single trial was calculated by multitaper spectral analysis (Thomson, 1982) in a given prestimulus window, and then averaged over the two selected S1 electrodes. To avoid the errorenous power estimation caused by a short window size, the prestimulus window was defined as (-500 ms, -20 ms). Here the number of tapers was three and the frequency resolution (zero-padding used) was 1 Hz. To normalize the inter-individual differences of prestimulus mu power, the trials were rank ordered by averaged prestimulus band power in the mu frequency range and then sorted into groups whose size corresponded to 10 % of the total trials, starting with the smallest prestimulus mu power and proceeding to the largest, and each group had 5 % of trials overlapped with the previous one.

For each power group, the probability of behavior detection was calculated and somatosensory N1 amplitude was averaged within 40 ms window centering on the maximum negative deflection of averaged SEP in 110–170 ms for each individual. Similarly, detection rates and N1 amplitudes for each power group were normalized as the percentage change of the mean values for each subject. Normalized detection rates and N1 amplitude were averaged across all subjects. The relationship between power group, normalized detection rates and N1 amplitudes were calculated. Statistical tests were based on ANOVA.

5.2.4 Granger Causality Spectral Analysis

Granger causality spectral analysis (Geweke, 1982; Ding et al., 2006) was applied to measure the directional influences among several cortical regions. First, we investigated the effect of the directional influences between frontal and S1 electrodes on behavioral performance.

An autoregressive model order was chosen for each individual by locating the minimum of the Akaike Information Criterion (Akaike, 1974). For each individual, Granger causality spectra were calculated in the prestimulus window for perceived and unperceived conditions, respectively.

Second, we investigated the relationship between N1 amplitude and the Granger causal influences between frontal and S1 cortical areas. For each individual, trials were grouped by the aforementioned approach. Granger causality spectra and N1 amplitude was calculated for each group subensemble, respectively. All the causality results were averaged over six site pairs between two electrodes in contralateral S1 areas and three in prefrontal areas.

Third, the relationship between the Granger causal influences from frontal to contralateral S1 cortical areas and prestimulus mu power was investigated. For each individual, all trials were sorted by prestimulus mu power and ten subensemble groups were resulted. Granger causality spectral analysis was applied in each subensemble group. Statistical tests were based on ANOVA.

5.3 Results

5.3.1 Behavioral Results

Trials having incorrect responses or incorrect response time (<0.15 s or >2.5 s) were less than 1%. Median response time over all thirteen subjects was 612 ± 35 ms (Mean $\pm$ SEM). After data preprocessing, each subject had at least 280 trials.

The histogram in Figure 5-2 A shows the probability of detecting a near-threshold stimulus for each individual. The grand average probability of detecting a stimulus over all subjects was 0.51 ± 0.01 (mean $\pm$ SEM) and it was not significantly different from 0.50 (student t test, $t = 1.33$, $p = 0.21$). Figure 5-2 B shows the probability of detecting stimuli as a function of time (around 5 min per block) and it was also not significantly different from 0.50 (student t test,

$t = -0.02$, $p = 0.98$) even though it was more variable in the last two or three blocks. These behavioral results suggest that, in the present EEG experiment, the probability of detecting a near-threshold electrical stimulus was kept around 0.50 and did not change significantly across subjects or over time.

5.3.2 Evoked Potentials

Figure 5-3 A shows the grand average SEP waveforms (0–200 ms) for perceived and unperceived conditions. In the present study, the scalp-recorded SEPs for perceived conditions have three main components: N20 (20–24 ms), P60 (50–70 ms), and N140 (120–160 ms). N20 component was not prominent due to the small intensity of the stimulus used in this EEG experiment and it was also distorted by the filtering of stimulation artifacts. The mean amplitudes of the positive deflection P60 didn't show significant differences (paired t test, $t = -1.81$, $p > 0.05$) between perceived and unperceived conditions. In contrast, N140 component was significantly enhanced (paired t test, $t = -8.25$, $p < 0.00002$) for perceived conditions, compared with unperceived conditions. These ERP results were consistent with previous ERP findings (Libet et al., 1967; Ray et al., 1999; Meador et al., 2002; Schubert et al., 2006), which suggested that SEPs (< 100 ms) were not significantly different between conscious and unconscious experiences. The two SEP components—N80 and P100 only appeared in three subjects and thus they were not discussed here.

Figure 5-3 B depicts 3D scalp current density maps of grand average SEPs at 60 ms and 140 ms. Current sources or sinks are indicated in red or blue, respectively. A dipolar pattern was shown at 60 ms, a current source in post-gyrus area and a current sink in pre-gyrus area. N1 component at 140 ms—a current sink, was displayed in broad cortical areas, including pre-gyrus areas, post-gyrus areas, and secondary somatosensory cortex.

5.3.3 Correlation of Prestimulus Mu Power and N1 Amplitude

Figure 5-1 shows that ongoing neural activity in contralateral S1 was dominated by mu rhythm whereas the higher frequency neural oscillations (> 20 Hz) were not salient in contralateral S1, a finding in agreement with previous studies (Salmelin and Hari, 1994). All thirteen subjects had prominent mu power peaks over contralateral S1, with peak frequencies from 9 to 11 Hz (mean: 10.5 ± 0.66 Hz).

The relationship between prestimulus mu power and N1 amplitude was calculated for each subject. Figure 5-4 shows an example of the relationship between prestimulus mu power and N1 amplitude for one subject's data set. Averaged SEPs (-500 ms, 200 ms) for ten power groups were shown in ascending order from top to bottom. Each group was averaged over 30 trials and two contralateral S1 electrodes. Averaged prestimulus waveforms have prominent mu oscillations in group 9 and 10. It is clear that the middle power groups (e.g., Group 6 or 7) have biggest N1 amplitude, whereas the largest or smallest power groups have smallest N1 amplitude.

In nine of thirteen subjects, the relationships between prestimulus mu power and N1 amplitude were well described by a quadratic regression model ($r^2 > 0.56$, $p < 0.05$) and were poorly described by a linear regression model ($r^2 < 0.22$, $p > 0.17$) (Figure 5-5 A). Figure 5-5 B shows an example of the inverted-U relationship (quadratic fit, $r^2 = 0.76$, $p < 0.006$) in one subject. By contrast, the relationships in three subjects were significantly positive or negative (Figure 5-5 C-D). No significant relationships were found in subject 2.

The correlations between prestimulus mu power and N1 amplitudes were averaged across all thirteen subjects. Figure 5-6 A shows that the level of prestimulus mu power was correlated with the probability of detecting stimuli in a parabolic way ($r^2 = 0.88$, $p < 0.0006$), which was in line with the findings in Linkenkaer-Hansen's paper (2004). The unfilled dots indicate the

change of grand average detection rate across all thirteen subjects for each group and the solid

curve indicates a quadratic regression fit for the data. The horizontal axis indicates the

percentage of prestimulus mu power. The vertical bar is the standard error of mean. The unequal

relationship was poorly described by a linear regression model ($r^2 = 0.32$, $p = 0.1$).

Figure 5-6 B shows that the relationship between prestimulus mu power and N1

amplitude from only perceived conditions was better described in a parabolic way ($r^2 = 0.88$, p

< 0.0006) and was poorly described by a linear regression ($r^2 = 0.01$, $p = 0.78$). Due to the lack

of N1 amplitude in unperceived conditions, only perceived conditions were used in the

following. N1 amplitudes in the intermediate power group increased 32% ± 17% (mean ± SEM)

or 44% ± 19% (mean ± SEM) respectively, compared with those in the lowest and highest power

groups.

5.3.4 Granger Causality Influences between PFC and S1

The Granger causality spectra were calculated between prefrontal and contralateral S1

electrodes for perceived and unperceived conditions, respectively. Figure 5-7 shows the Granger

causality spectra between prefrontal and contralateral S1 cortical areas for one subject's data set.

The Granger causality spectra from PFC to S1 were much enhanced in mu range (peak at 10 Hz,

0.17) for perceived conditions, compared with those (peak at 10 Hz, 0.05) for unperceived

conditions. In constrast, the spectra from S1 to PFC had smaller values (< 0.05) and didn't show

differences between perceived and unperceived conditions. In addition, the Granger causality

values in the beta and gamma bands (20–40 Hz) were small.

Hence, to achieve better comparisons, the Granger causality spectra were averaged in mu

band for perceived and unperceived conditions, respectively. To remove the variability from

different subjects, the averaged Granger causality values were normalized to (0, 1), namely, the

value (x or y) estimated from perceived or unperceived trials divided by the summed value (x + y), respectively. The Granger causal influences for perceived conditions were significantly stronger (paired t-test, $t = 3.89$, $p < 0.002$) than those for unperceived trials (Figure 5-8 A). However, the directional influences from S1 to PFC cortical areas were found to be not significantly different (paired t-test, $t = 0.62$, $p = 0.55$) between perceived and unperceived conditions and were also inconsistent across subjects (Figure 5-8 B). Six of thirteen subjects had higher causal influences from S1 to PFC for perceived conditions whereas the other seven subjects had higher causal influences from S1 to PFC for unperceived conditions.

Given the evidence of the effect of top-down attentional control on the N1 amplitude, the Granger causal influences from PFC to S1 were predicted to be positively correlated with the N1 amplitude. Due to the lack of N1 in unperceived trials, only perceived trials were used here. The Granger causality analysis was applied in each aforementioned subensemble group. To remove the variability of each individual, Granger causality and N1 amplitude both were normalized to (0, 1). Figure 5-9 shows that the relationship between the directional influences from PFC to S1 cortical areas and N1 amplitude was significantly positive (Spearman, $\rho = 0.79$, $p < 0.005$).

The nine subjects having the inverted-U relationship were selected. Trials, including perceived and unperceived trials, were sorted by prestimulus mu power. The Granger causality analysis was applied in each subensemble group. Figure 5-10 A shows that the highest directional influences from PFC to contralateral S1 were significantly (quadratic fit, $r^2 = 0.81$, $p < 0.003$) correlated with the intermediate level of prestimulus mu power. Figure 5-10 B shows an example of the inverted-U relationship (quadratic fit, $r^2 = 0.73$, $p < 0.01$) estimated from subject 10. In constrast, subject 4 or 13 have positive (linear regression fit, $r^2 = 0.75$, $p < 0.001$) or negative (linear regression fit, $r^2 = 0.48$, $p < 0.03$) relationships, respectively (Figure 5-10 C)

and D). These relationships are in line with the aforementioned relationships between prestimulus mu power and N1 amplitude.

We did several extra studies. First, we investigated the Granger causal influences in higher frequency range (> 16 Hz and < 45 Hz) and no significant results were found. In the present study, only the consistent results about Granger causal influences in mu band from PFC to contralateral S1 cortical areas were found. Second, we changed the prestimulus window to (-600 ms, -20 ms) or (-400 ms, -20 ms) and then recalculated the aforementioned correlations and Granger causality influences. The results for different prestimulus time windows didn't show significant differences. Third, to explore the effect of other cortical areas on contralateral S1, we selected the posterior parietal cortex (PPC), which is important in sensory integration, and investigated the directional influences from posterior parietal cortex to contralateral S1. No significant differences ($p = 0.12$) between perceived and unperceived conditions were found (Figure 5-11 A). Fourth, we also investigated the Granger causal influences from PFC to occipital cortex. The results didn't show significant differences ($p = 0.17$) between perceived and unperceived conditions (Figure 5-11 B).

5.4 Discussion

In our study, we investigated the effects of ongoing mu oscillations on behavioral detection of a weak stimulus and stimulus evoked N1 amplitude. An intermediate amount of prestimulus mu power was significantly correlated with enhanced sensory processing to a weak stimulus. We also investigated the impacts of the top-down attentional influences on sensory processing and N1 amplitude. We found that the top-down influences in mu band from prefrontal and other frontal structures to S1 were stronger for perceived trials than those for unperceived trials and was positively correlated with N1 amplitude. These higher order frontal structures

exert the top-down excitatory or inhibitory influences on posterior sensory cortices and mediate them in the optimal state to sensory input and thus facilitate subsequent sensory processing.

5.4.1 Spontaneous Membrane Potentials and Sensory Processing

Scalp EEG signals reflect the oscillations of postsynaptic potentials of neocortex, which are synchronized across several centimeters (Nunez et al., 2001). Postsynaptic potentials are membrane potential changes of postsynaptic terminals of a synapse. The frequency characteristics of scalp EEG depend on the membrane properties and their intrinsic network organization (da Silva, 1991).

At a cellular level, both the phase and amplitude of membrane potential oscillations (MPOs) are reported to significantly affect sensory processing. Numerous *in vitro* or *in vivo* studies demonstrated that spontaneous membrane potential fluctuations, especially the large amplitude oscillations in 5–20 Hz, carried significant temporal information and thus influenced the timing of action potential firing and integration of sensory input (Lampl and Yarom, 1993; Desmaisons et al., 1999; Schaefer et al., 2006). Schaefer et al. (2006) showed that sensory input could be robustly perceived when external stimulus input arrived at the trough and early rising phase of MPOs, which was remarkably in line with the scalp EEG findings of Jansen and Brandt (1991).

However, the effect of the amplitude of MPOs on sensory processing is still in active debate. There are three different hypotheses about the interaction between spontaneous membrane potential fluctuations and sensory input. First, spontaneous MPOs were thought to reflect a depolarizing drive on principle cells (Azouz and Gray, 1999; Destexhe and Pare, 1999; McCormick et al., 2003; Shu et al., 2003; Vertes, 2005). Input-related release of glutamate, when coupled with episodes of spontaneous MPOs, leads to more vigorous activation. Thus, the

absence or very low levels of spontaneous activity fails to bring local neuron populations closer to firing threshold and thus results in weak subsequent sensory evoked responses.

In constrast, the excessive level of spontaneous MPOs has also been found to impair sensory processing by competing with sensory evoked responses (Destexhe et al., 2003; Petersen et al., 2003; Dehaene and Changeux, 2005; Schaefer et al., 2006). The high level of prolonged spontaneous membrane potential fluctuations increases the membrane conductance and thus causes spontaneous firing of action potentials prior to synaptic input. The prolonged periods of spontaneous firing preceding synaptic input result in short-term depression of excitatory synapses by depletion of synaptic vesicles (Abbott et al., 1997; Galarreta and Hestrin, 1998; Chung et al., 2002; Petersen, 2002; Zucker and Regehr, 2002). In addition, the activation of a subset of GABAergic interneurons surrounding the excitatory pyramidal neuronal populations enhances the inhibitory synaptic influences on sensory responses (Galarreta and Hestrin, 1998; Markram et al., 1998; Reyes et al., 1998).

Furthermore, recent slice and simulation studies have demonstrated that the moderate amount of spontaneous membrane potential fluctuations, not too small or too big, can make local neuron populations more sensitive to synaptic input, especially the small-amplitude input (Destexhe and Pare, 1999; Ho and Destexhe, 2000; Destexhe et al., 2001; Rudolph and Destexhe, 2001). The facilitating effect of these spontaneous background activities on stimulus processing is called intrinsic stochastic resonance, which is functionally similar to the stochastic resonance shown to enhance sensory detection by adding noise in a nonlinear system (Wiesenfeld and Moss, 1995; Ho and Destexhe, 2000; Stocks and Mannella, 2001).

Thus, the relationship between ongoing neural activity and sensory evoked responses may be not monotonically positive or negative. The intermediate level of the alpha or alpha-like

70

brain rhythms generated in sensory cortical areas is predicted to optimize stimulus processing to a weak stimulus. It also may explain the aforementioned inconsistent findings by other EEG research groups.

5.4.2 Somatosensory Evoked Potentials and Sensory Processing

Three SEP components-N20, P60, and N140 are known to have distinct neural origins and physiological characteristics and interact differently with prestimulus mu oscillations. N20 reflects a population EPSP generated from excitation of the basal dendrites of pyramidal neurons in area 3b (Wikstrom et al., 1996). P60 represents an IPSP near the somata of pyramidal cells in area 3b (Wikstrom et al., 1996; Huttunen et al., 2006). N20 and P60 components were reported to be not significantly correlated with prestimulus mu power (Nikouline et al., 2000) but varied with stimulus parameters (Lesser et al., 1979; Allison et al., 1992). Thus, N20 and P60 components are mainly exogenously determined components.

Somatosensory N1 component, accompanied by high firing rate of action potentials in layers IV-V (Kulics and Cauller, 1986; Cauller and Kulics, 1991), is generated in layer I/II of S1 by the interaction between the feedforward projections from S1 and the feedback projections from other higher order cortices, including S2, frontal areas, and posterior parietal cortex (Cauller and Kulics, 1991; Cauller, 1995; Cauller et al., 1998; Jackson and Cauller, 1998; Staines et al., 2002; Golmayo et al., 2003). N1 component is enhanced by both exogenous (e.g., stimulus intensity) and endogenous (e.g., attention) factors (Nakajima and Imamura, 2000). In the present study, N1 amplitude was mainly affected by endogenous not exogenous factors due to the small intensity of electrical stimuli.

Recently, a novel model linking ERP components (> 100 ms) to the N-methyl-D-aspartate (NMDA) receptors (Mccarley et al., 1991; da Rocha et al., 2001; Giaquinto and Fraioli, 2003) is supported by the fact that NMDA receptors mediate prolonged sensory evoked

71

responses (Armstrongjames et al., 1993; Salin and Bullier, 1995), whereas non-NMDA receptors (e.g., AMPA) modulate fast responses. NMDA receptors, denser in supragranular layer, have stronger influences on cortical feedback projections (Fox et al., 1989). In addition, it has been demonstrated that spontaneous neural oscillations in the 8–14 Hz range were NMDA receptor-dependent (Silva et al., 1991; Flint and Connors, 1996). Thus, both prestimulus mu oscillations and N1 component are NMDA receptor-dependent, whereas, as aforementioned, N20 and P60 are mostly generated in infragrandular layers. Altogether, it is not surprising that prestimulus mu oscillations significantly affect N1 component, not early evoked responses — N20 or P60.

5.4.3 Top-down Attentional Control on Sensory Processing

Anatomical evidence and numerous physiological studies (Fuster, 2001) suggest that the prefrontal cortex is the highest level of the sensorimotor hierarchy, which mediates the top-down control by sending modulatory 'bias signals' to lower-order circuits and priming sensorimotor information processing. Engel et al. (2001) considered that synchronous neural oscillations, carrying these modulatory bias signals, were important in the top-down processing. Summarizing previous experimental and modeling studies, a recent hypothesis postulates that the lower frequency synchronization, due to long conduction delays, are more likely acclimated to the large-scale top-down processing (Kopell et al., 2000; von Stein et al., 2000; Engel et al., 2001; Buschman and Miller, 2007).

Recently, a growing number of studies demonstrated that mu (or alpha) band neural synchronization in frontal-parietal networks plays a significant role in cognitive attentional tasks by calculating coherence, Granger causality and, phase synchronization (Kaminski et al., 2001; Halgren et al., 2002; Jensen et al., 2002; Hesse et al., 2003; Yamagishi et al., 2003; Serrien et al., 2004; Palva et al., 2005; Sauseng et al., 2005a; Sauseng et al., 2005b). The top-down control can act either before or after a stimulus. In particular, during anticipation or expectancy, the top-

down factors can significantly enhance subsequent sensory processing in posterior sensory cortices (Engel and Singer, 2001; Fries et al., 2001; Super et al., 2003; Palva et al., 2005). In our present study, the top-down influences, indicated by the Granger causality spectra from frontal to posterior sensory cortical areas, imply that the prefrontal cortex sets up a brain state in posterior sensory areas that facilitates the detection of weak stimuli, further supporting these findings.

Somatosensory N1 component is historically known to be enhanced by the top-down signals exerted from the anterior attention system, such as, prefrontal cortex and anterior cingulate cortex (Posner and Petersen, 1990; Waberski et al., 2002). Conversely, neurological patients with prefrontal damage were observed to have attention deficits, which markedly reduce N1 amplitude (Knight, 1997; Chao and Knight, 1998; Knight et al., 1999). Hence, the robust positive relationship between N1 amplitude and the directional influences from frontal areas to S1 suggests that prefrontal and other higher order areas send bias signals to S1 and then modulate spontaneous mu oscillations to the optimal intermediate level, which is conducive to sensory processing to a weak stimulus.

In addition, during ongoing periods, the top-down attentional influences have been shown to significantly affect the levels of spontaneous neuronal activation at an attended or non-attended location (Kastner et al., 1999; Smith et al., 2000). However, there is a discrepancy about the relationship between attention and spontaneous neural activation (Luck et al., 1997; McAdams and Maunsell, 1999). Luck et al. (1997) reported that when attention was shifted to a particular stimulus location the spontaneous firing rate increased >30% in the same area. On the other hand, McAdams and Maunsell (1999) reported the baseline activity didn't change with attention shift.

Furthermore, our study examined the relationship between the top-down attentional influences and spontaneous neural activation levels in a more detailed quantitative analysis. Our findings raise the possibility that preceding sensory input the facilitatory top-down modulation from prefrontal cortex to primary somatosensory cortex is associated with the optimal level of prestimulus mu oscillations. Figure 5-10 A shows that the intermediate level of ongoing mu oscillations is correlated with the strongest top-down causal influences, whereas the highest or lowest oscillations are correlated with the weakest top-down influences. This physiological phenomenon supports the hypothesis postulated by Knight and his colleagues (Knight et al., 1999) that prefrontal cortex exerts parallel excitatory and inhibitory modulations of neural activity over posterior sensory and association cortices.

Cortical oscillatory activity is thought to reflect the excitation level of cortical areas (Fries, 2005). The highest level of prestimulus mu oscillations in primary somatosensory cortex suggests the highest excitation level, accompanied by the most vigorously firing, which is the result of a lack of inhibitory regulation from prefrontal cortex and other frontal cortical areas. On the other hand, the lowest level implies that there is a lack of excitatory regulation in S1. Hence, the weak top-down influences result in too much or too small excitation in posterior sensory cortices and thus reduce the efficacy of stimulus processing, whereas through the balanced excitatory and inhibitory regulation from prefrontal cortex the strong top-down influences modulate posterior sensory areas to the intermediate excitation level and thus facilitate stimulus processing.

Two remarks are in order. During ongoing periods, the fact that the prefrontal and other frontal structures, not posterior parietal cortex, effectively exert the top-down influences on S1 suggests the prefrontal and other frontal structures are crucial in subsequent sensory processing.

74

Second, the fact that the prefrontal cortex has little influences on the occipital cortex suggests that somatosensory perception is enhanced by the higher top-down influences on S1, not simply affected by the increased level of arousal.

In summary, our findings suggest that there exists an optimal intermediate level of spontaneous neural oscillations (~10 Hz) in posterior somatosensory cortex for late enhanced sensory responses to a weak stimulus. Prefrontal cortex and other higher-order structures, via ongoing neural oscillations, exert cognitive attentional control over posterior somatosensory cortical areas, modulate spontaneous mu oscillations in the optimal level, and thus improve behavioral performance and somatosensory N1 amplitude.
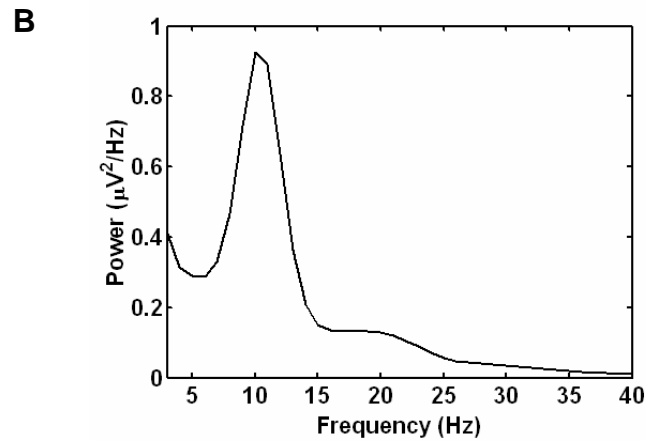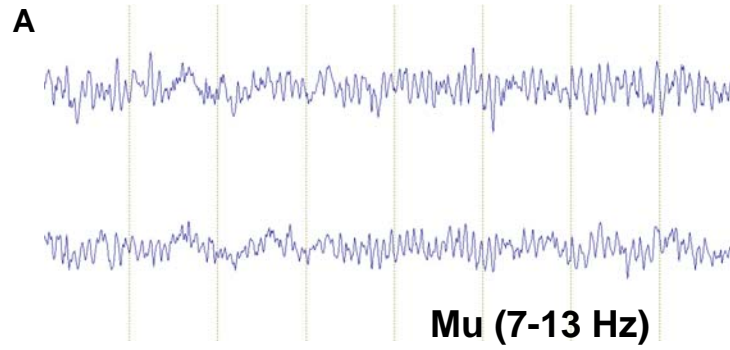
Figure 5-1. Characteristics of spontaneous mu oscillations. A) Examples of spontaneous mu oscillations recorded from two EEG electrodes over contralateral S1 cortical areas. The length of EEG traces is 8 sec. B) Grand average prestimulus power spectra (3-40 Hz) over contralateral S1.
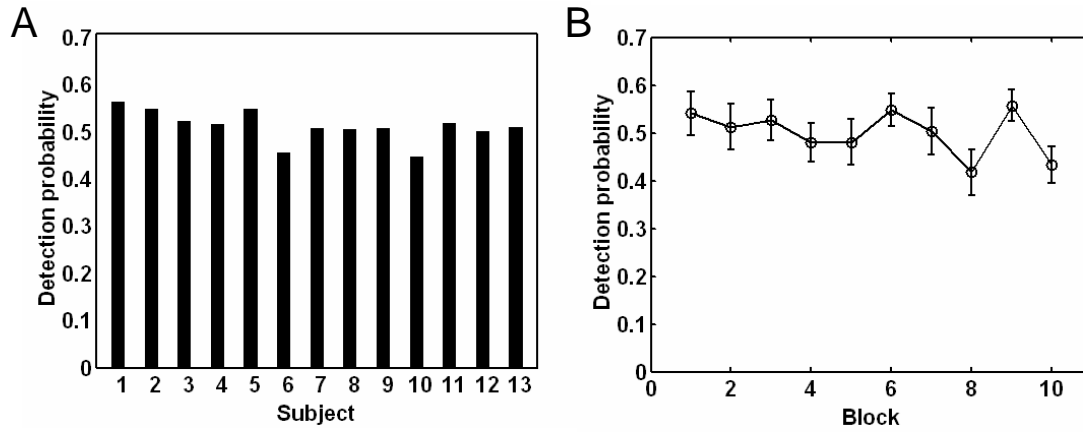
Figure 5-2. Behavioral performance in a somatosensory perception task. A) The histogram bars show the probability of detecting a near-threshold electrical stimulus for each individual. The grand average probability over all thirteen subjects is 0.51. B) The probability of detecting a stimulus was estimated in each block and averaged across all thirteen subjects. Error bars are standard error of mean.
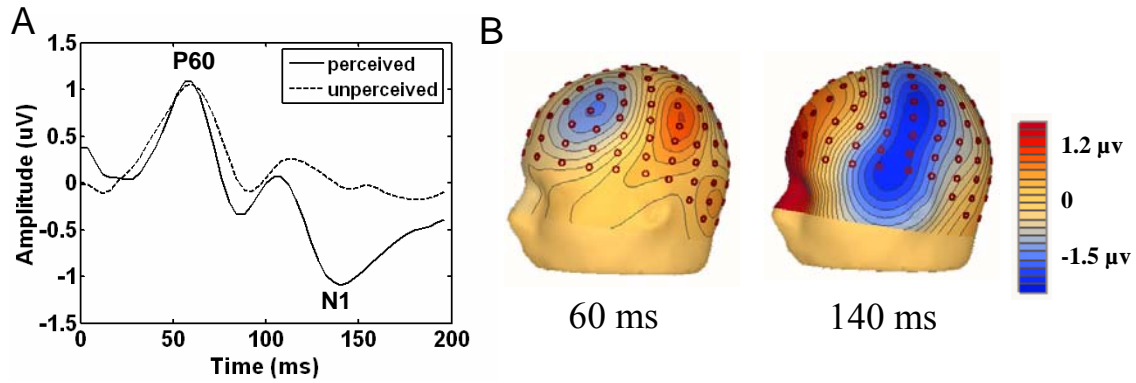
Figure 5-3. Characteristics of somatosensory evoked potentials in a somatosensory perception task. A) Grand average SEPs for perceived (solid curve) and unperceived (dotted curve) trials in contralateral S1. Positivity is represented as an upward deflection. N1 component was significantly enhanced for perceived trials. B) Scalp current source density maps of grand average SEPs at 60 ms and 140 ms in left hemisphere. Locations of 128-channel EEG recording electrodes are shown by red dots.
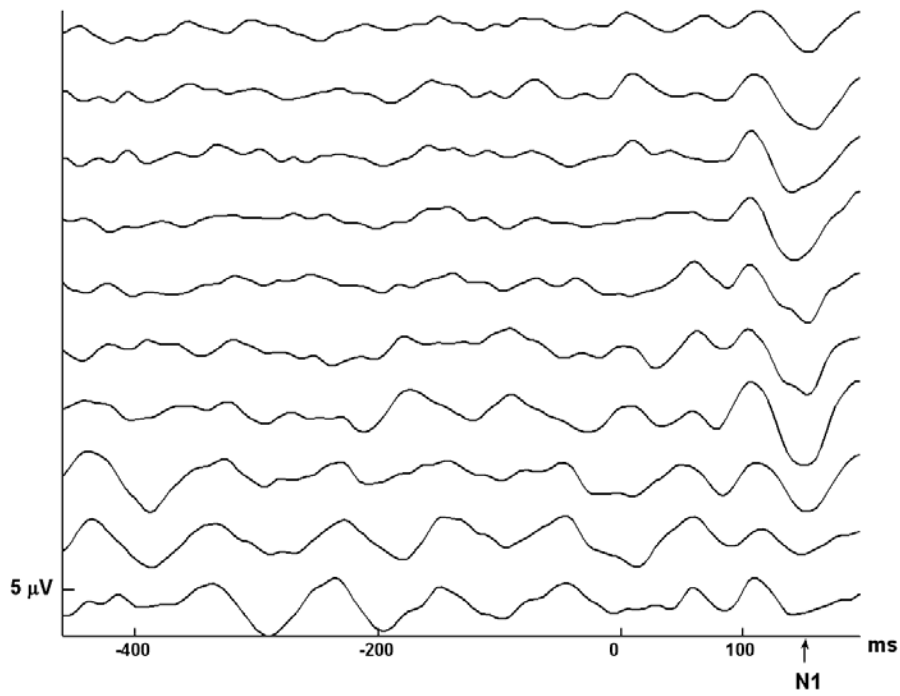
Figure 5-4. Averaged somatosensory evoked potentials for ten power groups. The averaged SEPs (-500 ms, 200 ms) were calculated from one subject's data set. Prestimulus mu power increases from top to bottom. The arrow indicates the peak latencies of N1 component.
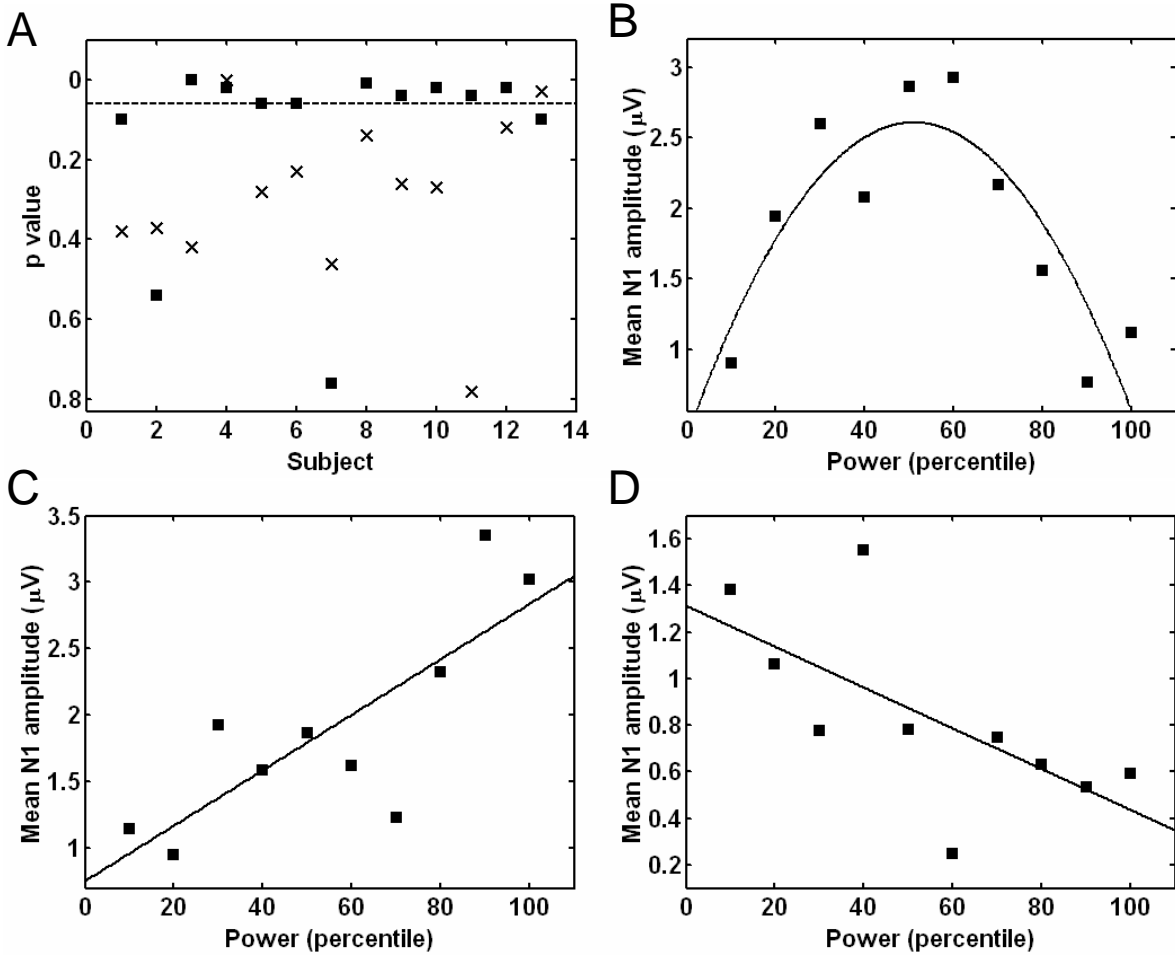
Figure 5-5. Regression data fit for all thirteen subjects. A) p value for all quadratic and linear regression fits. The horizontal dotted line indicates the significance level $p = 0.05$. The filled square indicates a quadratic regression fit and the symbol "x" means a linear regression fit. The relationship between prestimulus mu power and N1 amplitude is an inverted-U shape (B, quadratic fit, $r^2 = 0.76$, $p < 0.006$) in subject 10, positive (C, linear regression fit, $r^2 = 0.64$, $p < 0.005$) in subject 4, and negative (D, linear regression fit, $r^2 = 0.45$, $p < 0.02$) in subject 13.
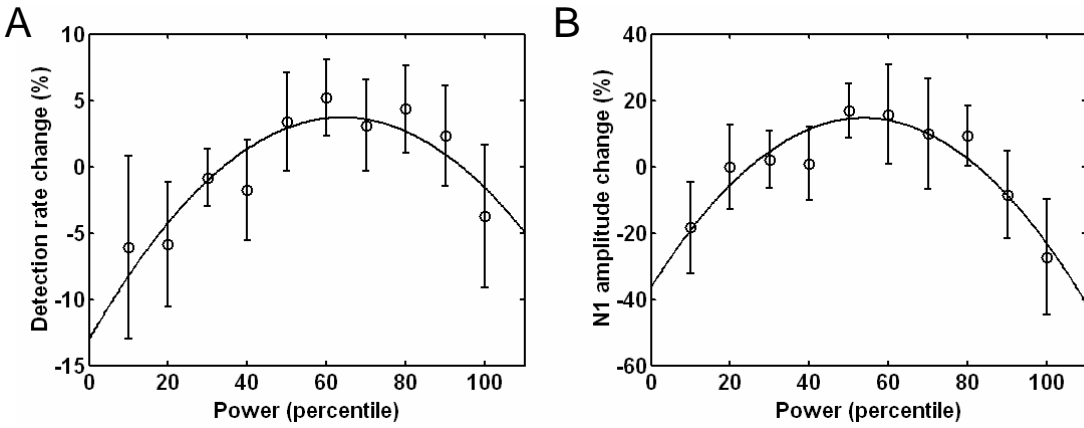
Figure 5-6. Prestimulus mu oscillations facilitate somatosensory perception. A) An inverted-U relationship (quadratic fit, $r^2 = 0.88$, $p < 0.0006$) exists between prestimulus mu power and the probability of detection rates. B) The relationship between prestimulus mu power and N1 amplitude is also an inverted-U shape (quadratic fit, $r^2 = 0.88$, $p < 0.0006$). Only perceived trials were used here. Error bars are standard error of mean.
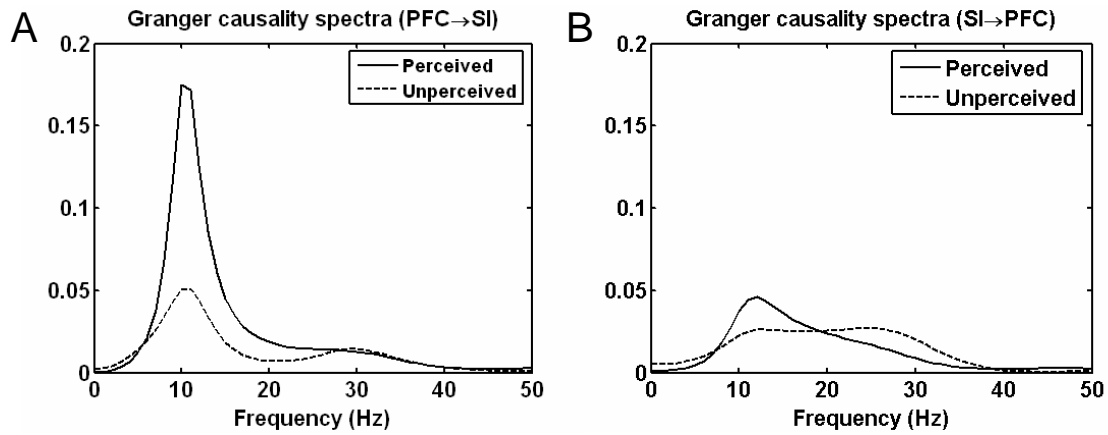
Figure 5-7. An example of Granger causality spectra between prefrontal and contralateral S1 cortical activities. A) Granger causality spectra from prefrontal to contralateral S1 cortical areas. B) Granger causality spectra from contralateral S1 to prefrontal cortical areas. Those for perceived conditions were shown in solid curves and those for unperceived conditions in dashed curves.
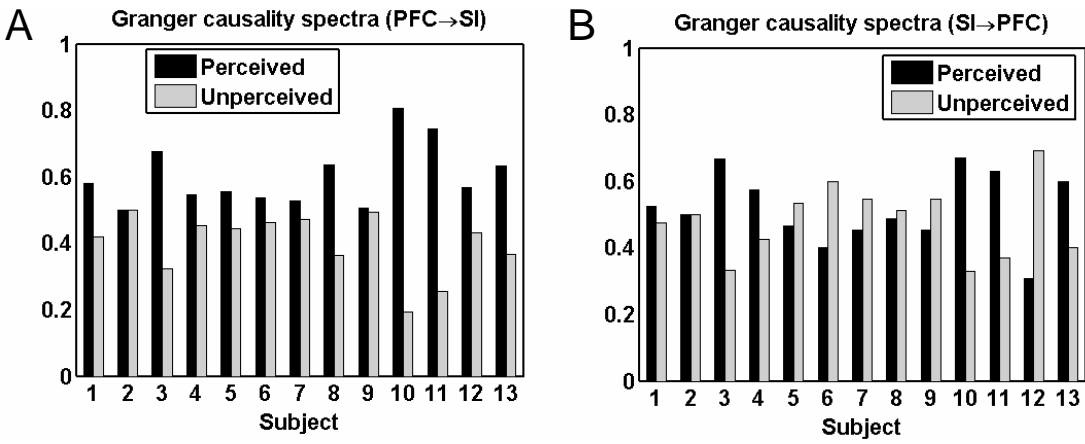
Figure 5-8. Granger causality influences between prefrontal and contralateral S1 cortical areas. Granger causality spectra were averaged in mu frequency range for each individual. A) The histogram shows that the Granger causality influences from prefrontal to contralateral S1 cortical activity are significantly (paired *t*-test, $p < 0.002$) stronger for perceived (black bars) conditions than those for unperceived (grey bars) conditions. b) The directional influences from contralateral S1 to PFC cortical activity are not significant different (paired *t*-test, $t = 0.62$, $p = 0.55$) between two conditions.
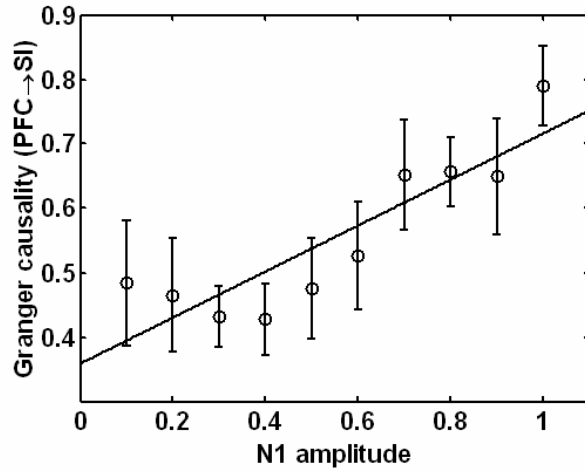
Figure 5-9. Relationship between the Granger causal influences from prefrontal to S1 cortical areas and N1 amplitude.
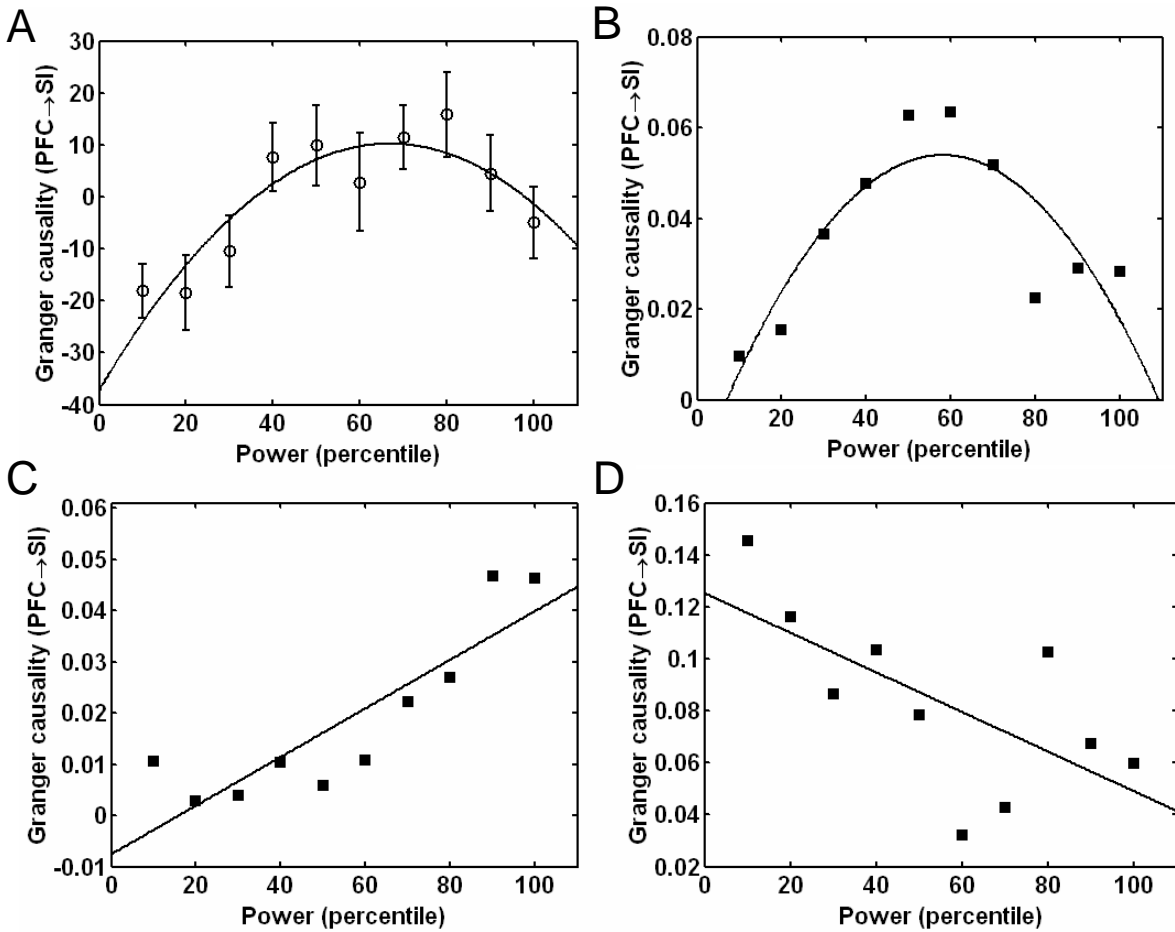
Figure 5-10. Relationships between prestimulus mu power and the Granger causality influences from prefrontal to contralateral S1 cortical areas. A) An inverted-U relationship (quadratic fit, $r^2 = 0.81$, $p < 0.003$) exists between prestimulus mu power and the causal influences from PFC to contralateral S1. B) An example of the inverted-U relationship (quadratic fit, $r^2 = 0.73$, $p < 0.01$) estimated from subject 10. Subject 4 and 13 have positive (C, linear regression fit, $r^2 = 0.75$, $p < 0.001$) or negative (D, linear regression fit, $r^2 = 0.48$, $p < 0.03$) relationships, respectively.
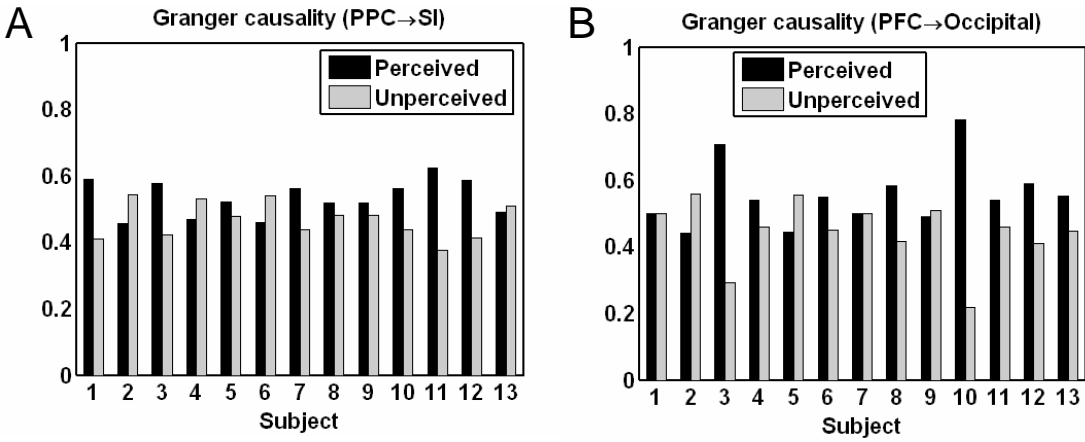
Figure 5-11. Granger causal influences between different cortical areas. A) The Granger causal influences from posterior parietal cortex to contralateral S1 cortical areas are not significantly ($p = 0.12$) different between perceived and unperceived conditions. B) Those from prefrontal to occipital cortical areas didn't show significantly differences ($p = 0.17$).

CHAPTER 6
CONCLUSIONS AND FURTURE RESEARCH

6.1 Conclusion

The brain is not a passive or stimulus driven system but an active and adaptive system. According to the intrinsic cortical signals reflecting previous experience, anticipation, and prediction, the brain can be modulated to the optimal state to facilitate the sensory and motor responses to external stimuli. In the cortical hierarchy, the higher order cortical areas, such as, prefrontal cortex and anterior cingulate cortex, are dedicated to play this functional role. They generate the intrinsic bias signals and send them to the lower order cortical areas, such as, primary sensory cortices, and further mediate the ongoing state in primary sensory and association cortices. Such top-down processing has been found before and after stimulus presentation in various cognitive attentional tasks (Engel et al., 2001).

The neural communication among different cortical areas is believed to interact effectively through synchronous neural oscillations (Engel et al., 2001; Fries, 2005). Fries (2005) proposed that coherent neural oscillations can cause a communication window for sensory input and output in different cortical areas to open at the same time, whereas weak incoherent neural oscillations lose the timing for input or output.

Hence, first, we investigated the effect of neural oscillations in different cortical areas on behavioral performance and sensory perception. Second, we applied adaptive multivariate autoregressive spectral analysis to investigate the characteristics of coherence and Granger causality of neural oscillations in sensorimotor integration and sensory perception. Our main findings are threefold: (1) in monkeys, depending on the brain region and frequency band, prestimulus oscillations are either significantly negatively correlated with RT or positively correlated with RT; (2) in monkeys and in humans, synchronized cortical sensorimotor networks

are bound together by mu or beta oscillations subserving sustained motor output during hold periods; (3) in humans, during the prestimulus interval, top-down attentional influences exerted from prefrontal and other frontal cortical structures can bring the posterior sensory neural activities to the optimal level for enhanced stimulus processing and behavioral performance. Together, these results demonstrate that ongoing neural oscillations play crucial roles in sensorimotor behavior in both humans and nonhuman primates.

6.2 Future Research

The future research has three aspects. In Chapter 5, the scalp EEG experiment was designed to explore the neural correlates of somatosensory processing to a weak stimulus. It has a lack of attention control and may be more or less affected by the level of arousal or other cognitive factors even though it was proven that the arousal level has insignificant effects on the EEG task. Thus, to extensively investigate the top-down attention control on somatosensory processing, well-designed attention conditions where the same stimulus can be either attended to or ignored, need to be added in future EEG experiments.

Another facet of my future research is source localization of ongoing neural oscillations. Nunez et al. (1997) pointed out that the approach to calculate coherence on raw scalp EEG data has a few pitfalls, including common reference and volume conduction. The effect of common reference or volume conduction can be effectively removed by applying average reference or Laplacian approach, respectively. However, the Laplacian and other high-resolution methods may underestimate the coherence and Granger causality by spatial filtering (Nunez et al., 1997; Nunez et al., 1999). Thus, to remove the impact of volume conduction effectively, it is better to localize the distinct underlying sources and apply the aforementioned spectral analysis on the source level. Thus, several source localization algorithms, including minimum-norm and beamforming techniques, will be applied in the future research.

Third, the current way to localize the neural activity in a distributed source model (e.g., sLORETA) has methodological difficulties, causing the mislocalization of sources, such as ghost sources and lost sources (Menendez and Andino, 2000). Additionally, some studies showed that these methods have difficulties to locate the deep sources, such as anterior cingulate cortex (Gomez et al., 2006). One possibility to constrain the solutions of source localization of EEG/MEG signals is the utilization of fMRI (Ritter and Villringer, 2006). Thus, our further study will coregister EEG with fMRI to localize the underlying sources more accurately.

APPENDIX A
MULTITAPER SPECTRAL ANALYSIS

The multitaper algorithm is a nonparametric method designed for very short-time data segments. The multitaper spectrum is estimated by averaging multiple windowed faster Fourier transforms generated with multiple orthogonal data tapers, particularly discrete prolate spheroidal sequences.

Let $x(t)$ be a zero mean, stationary random process, $t = 1, 2, \cdots, N$, and $w_t(k)$, $k = 1, 2, \cdots, K$, are the orthogonal taper functions. The Fourier transform of $x(t)$ is defined in Equation A-1. The Fourier transform of the data sequences can be obtained through Equation A-2 and A-3.

$$x(t) = \int_{-1/2}^{1/2} dX(f) e^{i2\pi ft} \tag{A-1}$$

$$\tilde{x}(f) = \sum_{j}^{N} x(t) e^{-i2\pi ft} = \int_{-1/2}^{1/2} K(f - f', N) dX(f') \tag{A-2}$$

$$K(f - f', N) = e^{-i2\pi(f-f')} \frac{N+1}{2} \frac{\sin(N\pi(f-f'))}{\sin(\pi(f-f'))} \tag{A-3}$$

The general multitaper spectrum estimate is:

$$S(f) = \frac{1}{K} \sum_{k=1}^{K} \left| \tilde{x}_k(f)^2 \right| \tag{A-4}$$

$$\tilde{x}_k(f) = \sum_{1}^{N} w_t(k) x_t e^{-i2\pi ft} \tag{A-5}$$

APPENDIX B
SECOND ORDER BLIND IDENTIFICATION

Second-order blind identification (SOBI) is a blind source separation method that estimates a joint diagonalizer of a set of covariance matrix by minimizing joint diagonalization (JD) criterion over the set of covariance matrices in order to separate temporally correlated signals and reduce noise effect.

SOBI enables the decomposition of n-channel continuous EEG and MEG signals into m SOBI components ($m \leq n$). Let $x(t)$ represent the measured n-channel EEG time series and $s(t)$ represent the m unknown underlying sources. $x(t)$ is an instantaneous linear mixture of source signals $s(t)$, via an unknown mixing matrix A. To obtain the estimated source signals $s(t)$, an unknown mixing matrix W multiplies $x(t)$.

$$x(t) = [x_1(t), x_2(t), x_3(t), \cdots, x_n(t)]^T \tag{B-1}$$

$$s(t) = [s_1(t), s_2(t), s_3(t), \cdots, s_m(t)]^T \tag{B-2}$$

$$x(t) = As(t) \tag{B-3}$$

$$s(t) = Wx(t) \tag{B-4}$$

$$A = W^{-1} \tag{B-5}$$

The SOBI algorithm has two main steps: data whitening and joint approximate diagonalization. The first step is to whiten the measured data $x(t)$ (must be centered) by a whitening matrix P so that:

$$E[Px(t)x(t)^* P^H] = PR_x(0)P^H = PAA^H P^H = I \tag{B-6}$$

The second step is to compute a set of covariance matrix $R_x(\tau)$, and then look for a unitary matrix V to joint diagonalize the set of $R_x(\tau)$ by minimizing the JD criterion:

$$\sum_{\tau}\sum_{i\neq j}(V^T RV)^2_{ij} \hspace{4cm} \text{(B-7)}$$

After SOBI separation, each SOBI component has one time series $s_i(t)$ and one associated component scalp maps. If $\hat{A}$ is an estimated $n \ x \ n$ matrix, the columns of $\hat{A}$ are the component scalp maps. The SOBI separation of EEG here was done with the codes modified from EEGLAB.

LIST OF REFERENCES

1.   Abbott LF, Varela JA, Sen K, Nelson SB (1997) Synaptic depression and cortical gain control. Science 275:220-224.

2.   Akaike H (1974) New look at statistical-model identification. IEEE Trans on Automat Contr Ac19:716-723.

3.   Allison T, Mccarthy G, Wood CC (1992) The relationship between human long-latency somatosensory evoked-potentials recorded from the cortical surface and from the scalp. Electroencephalogr Clin Neurophysiol 84:301-314.

4.   Allison T, Mccarthy G, Wood CC, Darcey TM, Spencer DD, Williamson PD (1989) Human cortical potentials-evoked by stimulation of the median nerve .1. cytoarchitectonic areas generating short-latency activity. J Neurophysiol 62:694-710.

5.   Arieli A, Sterkin A, Grinvald A, Aertsen A (1996) Dynamics of ongoing activity: explanation of the large variability in evoked cortical responses. Science 273:1868-1871.

6.   Armstrongjames M, Welker E, Callahan CA (1993) The contribution of NMDA and non-NMDA receptors to fast and slow transmission of sensory information in the rat Sl barrel cortex. J Neurosci 13:2149-2160.

7.   Azouz R, Gray CM (1999) Cellular mechanisms contributing to response variability of cortical neurons in vivo. J Neurosci 19:2209-2223.

8.   Baker SN, Olivier E, Lemon RN (1997) Coherent oscillations in monkey motor cortex and hand muscle EMG show task-dependent modulation. J Physiol 501 (Pt 1):225-241.

9.   Baker SN, Kilner JM, Pinches EM, Lemon RN (1999) The role of synchrony and oscillations in the motor output. Exp Brain Res 128:109-117.

10.   Belouchrani A, AbedMeraim K, Cardoso JF, Moulines E (1997) A blind source separation technique using second-order statistics. IEEE Trans on Signal Proces 45:434-444.

11.   Berger H (1929) Electroencephalogram in humans. Arch Psychiatr Nervenkr 87:527-570.

12.   Bernier R, Dawson G, Webb S, Murias M (2007) EEG mu rhythm and imitation impairments in individuals with autism spectrum disorder. Brain Cogn 64:228-237.

13.   Bland BH, Konopacki J, Dyck RH (2002) Relationship between membrane potential oscillations and rhythmic discharges in identified hippocampal theta-related cells. J Neurophysiol 88:3046-3066.

14.   Brandt ME, Jansen BH, Carbonari JP (1991) Pre-stimulus spectral EEG patterns and the visual evoked-response. Electroencephalogr Clin Neurophysiol 80:16-20.

15. Brovelli A, Ding M, Ledberg A, Chen Y, Nakamura R, Bressler SL (2004) Beta oscillations in a large-scale sensorimotor cortical network: directional influences revealed by Granger causality. Proc Natl Acad Sci U S A 101:9849-9854.

16. Brown P (2000) Cortical drives to human muscle: the Piper and related rhythms. Prog Neurobiol 60:97-108.

17. Brunia CH (1999) Neural aspects of anticipatory behavior. Acta Psychol (Amst) 101:213-242.

18. Buschman TJ, Miller EK (2007) Top-down versus bottom-up control of attention in the prefrontal and posterior parietal cortices. Science 315:1860-1862.

19. Cauller L (1995) Layer I of primary sensory neocortex: where top-down converges upon bottom-up. Behav Brain Res 71:163-170.

20. Cauller LJ, Kulics AT (1991) The neural basis of the behaviorally relevant N1 component of the somatosensory-evoked potential in SI cortex of awake monkeys - evidence that backward cortical projections signal conscious touch sensation. Exp Brain Res 84:607-619.

21. Cauller LJ, Clancy B, Connors BW (1998) Backward cortical projections to primary somatosensory cortex in rats extend long horizontal axons in layer I. J Comp Neurol 390:297-310.

22. Chao LL, Knight RT (1998) Contribution of human prefrontal cortex to delay performance. J Cogn Neurosci 10:167-177.

23. Chatrian GE, Petersen MC, Lazarte JA (1959) The blocking of the rolandic wicket rhythm and some central changes related to movement. Electroencephalogr Clin Neurophysiol 11:497-510.

24. Chen R, Corwell B, Hallett M (1999) Modulation of motor cortex excitability by median nerve and digit stimulation. Exp Brain Res 129:77-86.

25. Chen Y, Bressler SL, Ding M (2006) Frequency decomposition of conditional Granger causality and application to multivariate neural field potential data. J Neurosci Methods 150:228-237.

26. Chung S, Li XR, Nelson SB (2002) Short-term depression at thalamocortical synapses contributes to rapid adaptation of cortical sensory responses in vivo. Neuron 34:437-446.

27. Conway BA, Halliday DM, Farmer SF, Shahani U, Maas P, Weir AI, Rosenberg JR (1995) Synchronization between motor cortex and spinal motoneuronal pool during the performance of a maintained motor task in man. J Physiol (Lond) 489:917-924.

28. da Rocha AF, Pereira A, Coutinho FAB (2001) N-methyl-D-aspartate channel and consciousness: from signal coincidence detection to quantum computing. Prog Neurobiol 64:555-573.

29. da Silva FHL (1990) A critical-review of clin-applications of topographic mapping of brain potentials. J Clin Neurophysiol 7:535-551.

30. da Silva FL (1991) Neural mechanisms underlying brain waves - from neural membranes to networks. Electroencephalogr Clin Neurophysiol 79:81-93.

31. Dehaene S, Changeux JP (2005) Ongoing spontaneous activity controls access to consciousness: A neuronal model for inattentional blindness. Plos Biol 3:910-927.

32. Desmaisons D, Vincent JD, Lledo PM (1999) Control of action potential timing by intrinsic subthreshold oscillations in olfactory bulb output neurons. J Neurosci 19:10727-10737.

33. Desmedt JE, Robertson D (1977) Differential enhancement of early and late components of cerebral somatosensory evoked-potentials during forced-paced cognitive tasks in man. J Physiol (Lond) 271:761-782.

34. Desmedt JE, Tomberg C (1989) Mapping early somatosensory evoked-potentials in selective attention - critical-evaluation of control conditions used for titrating by difference the cognitive P-30, P40, P100 and N140. Electroencephalogr Clin Neurophysiol 74:321-346.

35. Desmedt JE, Huy NT, Bourguet M (1983) The cognitive P40, N60 and P100 components of somatosensory evoked potentials and the earliest electrical signs of sensory processing in man. Electroencephalogr Clin Neurophysiol 56:272-282.

36. Destexhe A, Pare D (1999) Impact of network activity on the integrative properties of neocortical pyramidal neurons in vivo. J Neurophysiol 81:1531-1547.

37. Destexhe A, Rudolph M, Pare D (2003) The high-conductance state of neocortical neurons in vivo. Nat Rev Neurosci 4:739-751.

38. Destexhe A, Rudolph M, Fellous JM, Sejnowski TJ (2001) Fluctuating synaptic conductances recreate in vivo-like activity in neocortical neurons. Neuroscience 107:13-24.

39. Ding M, Chen Y, Bressler SL (2006) Granger causality: basic theory and application to neuroscience. In: Handbook of time series analysis (B. Schelter MW, and J. Timmer, ed), pp 437-460. Weinheim: Wiley-VCH Verlag.

40. Ding MZ, Bressler SL, Yang WM, Liang HL (2000) Short-window spectral analysis of cortical event-related potentials by adaptive multivariate autoregressive modeling: data preprocessing, model validation, and variability assessment. Biol Cybern 83:35-45.

41. Donchin E, Lindsley DB (1966) Average evoked potentials and reaction times to visual stimuli. Electroencephalogr Clin Neurophysiol 20:217-223.

42. Donoghue JP, Sanes JN, Hatsopoulos NG, Gaal G (1998) Neural discharge and local field potential oscillations in primate motor cortex during voluntary movements. J Neurophysiol 79:159-173.

43. Eckhorn R, Bauer R, Jordan W, Brosch M, Kruse W, Munk M, Reitboeck HJ (1988) Coherent oscillations: a mechanism of feature linking in the visual cortex? Multiple electrode and correlation analyses in the cat. Biol Cybern 60:121-130.

44. Engel AK, Singer W (2001) Temporal binding and the neural correlates of sensory awareness. Trends Cogn Sci 5:16-25.

45. Engel AK, Fries P, Singer W (2001) Dynamic predictions: oscillations and synchrony in top-down processing. Nat Rev Neurosci 2:704-716.

46. Flint AC, Connors BW (1996) Two types of network oscillations in neocortex mediated by distinct glutamate receptor subtypes and neuronal populations. J Neurophysiol 75:951-956.

47. Fox K, Sato H, Daw N (1989) The location and function of NMDA receptors in cat and kitten visual-cortex. J Neurosci 9:2443-2454.

48. Foxe JJ, Simpson GV, Ahlfors SP (1998) Parieto-occipital approximately 10 Hz activity reflects anticipatory state of visual attention mechanisms. Neuroreport 9:3929-3933.

49. Fries P (2005) A mechanism for cognitive dynamics: neuronal communication through neuronal coherence. Trends Cogn Sci 9:474-480.

50. Fries P, Neuenschwander S, Engel AK, Goebel R, Singer W (2001) Rapid feature selective neuronal synchronization through correlated latency shifting. Nat Neurosci 4:194-200.

51. Fuster JM (2001) The prefrontal cortex--an update: time is of the essence. Neuron 30:319-333.

52. Galarreta M, Hestrin S (1998) Frequency-dependent synaptic depression and the balance of excitation and inhibition in the neocortex. Nat Neurosci 1:587-594.

53. Garcia-Larrea L, Lukaszewicz AC, Mauguiere F (1995) Somatosensory responses during selective spatial attention - the N120-to-N140 transition. Psychophysiology 32:526-537.

54. Gastaut HJ, Bert J (1954) EEG changes during cinematographic presentation - (Moving picture activation of the EEG). Electroencephalogr Clin Neurophysiol 6:433-444.

55. Geweke J (1982) Measurement of linear dependence and feedback from multiple time series. J Am Stat Assoc 77:304-313.

56. Giaquinto S, Fraioli L (2003) Enhancement of the somatosensory N140 component during attentional training after stroke. Clin Neurophysiol 114:329-335.

57. Golmayo L, Nunez A, Zaborszky L (2003) Electrophysiological evidence for the existence of a posterior cortical-prefrontal-basal forebrain circuitry in modulating sensory responses in visual and somatosensory rat cortical areas. Neuroscience 119:597-609.

58. Gomez CM, Marco-Pallares J, Grau C (2006) Location of brain rhythms and their modulation by preparatory attention estimated by current density. Brain Res 1107:151-160.

59. Gonzalez Andino SL, Michel CM, Thut G, Landis T, Grave de Peralta R (2005) Prediction of response speed by anticipatory high-frequency (gamma band) oscillations in the human brain. Hum Brain Mapp 24:50-58.

60. Granger CWJ (1969) Investigating causal relations by econmetric models and cross-spectral methods. Econometrica 37:424-438

61. Gray CM, Singer W (1989) Stimulus-specific neuronal oscillations in orientation columns of cat visual cortex. Proc Natl Acad Sci U S A 86:1698-1702.

62. Gross J, Tass PA, Salenius S, Hari R, Freund HJ, Schnitzler A (2000) Cortico-muscular synchronization during isometric muscle contraction in humans as revealed by magnetoencephalography. J Physiol 527 Pt 3:623-631.

63. Haig AR, Gordon E (1998) Prestimulus EEG alpha phase synchronicity influences N100 amplitude and reaction time. Psychophysiology 35:591-595.

64. Halgren E, Boujon C, Clarke J, Wang C (2002) Rapid distributed fronto-parieto-occipital processing stages during working memory in humans. Cereb Cortex 12:710-728.

65. Halliday DM, Conway BA, Farmer SF, Rosenberg JR (1998) Using electroencephalography to study functional coupling between cortical activity and electromyograms during voluntary contractions in humans. Neurosci Lett 241:5-8.

66. Hesse W, Moller E, Arnold M, Schack B (2003) The use of time-variant EEG Granger causality for inspecting directed interdependencies of neural assemblies. J Neurosci Methods 124:27-44.

67. Ho N, Destexhe A (2000) Synaptic background activity enhances the responsiveness of neocortical pyramidal neurons. J Neurophysiol 84:1488-1496.

68. Homan RW, Herman J, Purdy P (1987) Cerebral location of international 10-20 system electrode placement. Electroencephalogr Clin Neurophysiol 66:376-382.

69. Houdayer E, Labyt E, Cassim F, Bourriez JL, Derambure P (2006) Relationship between event-related beta synchronization and afferent inputs: analysis of finger movement and peripheral nerve stimulations. Clin Neurophysiol 117:628-636.

70. Huttunen J, Komssi S, Lauronen L (2006) Spatial dynamics of population activities at S1 after median and ulnar nerve stimulation revisited: an MEG study. Neuroimage 32:1024-1031.

71. Jackson ME, Cauller LJ (1998) Neural activity in SII modifies sensory evoked potentials in SI in awake rats. Neuroreport 9:3379-3382.

72.   Jensen O, Gelfand J, Kounios J, Lisman JE (2002) Oscillations in the alpha band (9–12 Hz) increase with memory load during retention in a short-term memory task. Cereb Cortex 12:877-882.

73.   Kaminski M, Ding MZ, Truccolo WA, Bressler SL (2001) Evaluating causal relations in neural systems: Granger causality, directed transfer function and statistical assessment of significance. Biol Cybern 85:145-157.

74.   Kastner S, Pinsk MA, De Weerd P, Desimone R, Ungerleider LG (1999) Increased activity in human visual cortex during directed attention in the absence of visual stimulation. Neuron 22:751-761.

75.   Kekoni J, Hamalainen H, Saarinen M, Grohn J, Reinikainen K, Lehtokoski A, Naatanen R (1997) Rate effect and mismatch responses in the somatosensory system: ERP-recordings in humans. Biol Psychol 46:125-142.

76.   Kida T, Nishihira Y, Wasaka T, Nakata H, Sakamoto M (2004) Differential modulation of temporal and frontal components of the somatosensory N140 and the effect of interstimulus interval in a selective attention task. Cogn Brain Res 19:33-39.

77.   Kilner JM, Baker SN, Salenius S, Hari R, Lemon RN (2000) Human cortical muscle coherence is directly related to specific motor parameters. J Neurosci 20:8838-8845.

78.   Kilner JM, Salenius S, Baker SN, Jackson A, Hari R, Lemon RN (2003) Task-dependent modulations of cortical oscillatory activity in human subjects during a bimanual precision grip task. Neuroimage 18:67-73.

79.   Klimesch W (1999) EEG alpha and theta oscillations reflect cognitive and memory performance: a review and analysis. Brain Res Rev 29:169-195.

80.   Klimesch W, Sauseng P, Hanslmayr S (2007) EEG alpha oscillations: the inhibition-timing hypothesis. Brain Res Rev 53:63-88.

81.   Klimesch W, Doppelmayr M, Schwaiger J, Auinger P, Winkler T (1999) 'Paradoxical' alpha synchronization in a memory task. Cogn Brain Res 7:493-501.

82.   Knight RT (1997) Distributed cortical network for visual attention. J Cogn Neurosci 9:75-91.

83.   Knight RT, Staines WR, Swick D, Chao LL (1999) Prefrontal cortex regulates inhibition and excitation in distributed neural networks. Acta Psychol (Amst) 101:159-178.

84.   Kopell N, Ermentrout GB, Whittington MA, Traub RD (2000) Gamma rhythms and beta rhythms have different synchronization properties. Proc Natl Acad Sci U S A 97:1867-1872.

85.   Kraft GH, Aminoff MJ, Baran EM, Litchy WJ, Stolov WC, subcomm ASEP (1998) Somatosensory evoked potentials: Clin uses. Muscle Nerve 21:252-258.

86. Kuhlman WN (1978) EEG feedback training - enhancement of somatosensory cortical activity. Electroencephalogr Clin Neurophysiol 45:290-294.

87. Kuhn AA, Williams D, Kupsch A, Limousin P, Hariz M, Schneider GH, Yarrow K, Brown P (2004) Event-related beta desynchronization in human subthalamic nucleus correlates with motor performance. Brain 127:735-746.

88. Kulics AT, Cauller LJ (1986) Cerebral cortical somatosensory evoked-responses, multiple unit-activity and current source-densities - their interrelationships and significance to somatic sensation as revealed by stimulation of the awake monkeys hand. Exp Brain Res 62:46-60.

89. Lamme VAF, Roelfsema PR (2000) The distinct modes of vision offered by feedforward and recurrent processing. Trends Neurosci 23:571-579.

90. Lampl I, Yarom Y (1993) Subthreshold oscillations of the membrane-potential - a functional synchronizing and timing device. J Neurophysiol 70:2181-2186.

91. Ledberg A, Bressler SL, Ding MZ, Coppola R, Nakamura R (2007) Large-scale visuomotor integration in the cerebral cortex. Cereb Cortex 17:44-62.

92. Leek MR (2001) Adaptive procedures in psychophysical research. Percept & Psychophys 63:1279-1292.

93. Lesser RP, Koehle R, Lueders H (1979) Effect of stimulus-intensity on short latency somatosensory evoked-potentials. Electroencephalogr Clin Neurophysiol 47:377-382.

94. Liang H, Bressler SL, Ding M, Truccolo WA, Nakamura R (2002) Synchronized activity in prefrontal cortex during anticipation of visuomotor processing. Neuroreport 13:2011-2015.

95. Libet B, Alberts WW, Wright EW, Feinstei.B (1967) Responses of human somatosensory cortex to stimuli below threshold for conscious sensation. Science 158:1597-1600.

96. Linkenkaer-Hansen K, Nikulin VV, Palva S, Ilmoniemi RJ, Palva JM (2004) Prestimulus oscillations enhance psychophysical performance in humans. J Neurosci 24:10186-10190.

97. Luck SJ, Chelazzi L, Hillyard SA, Desimone R (1997) Neural mechanisms of spatial selective attention in areas V1, V2, and V4 of macaque visual cortex. J Neurophysiol 77:24-42.

98. MacKay WA, Mendonca AJ (1995) Field potential oscillatory bursts in parietal cortex before and during reach. Brain Res 704:167-174.

99. Makeig S, Westerfield M, Jung TP, Enghoff S, Townsend J, Courchesne E, Sejnowski TJ (2002) Dynamic brain sources of visual evoked responses. Science 295:690-694.

100. Markram H, Wang Y, Tsodyks M (1998) Differential signaling via the same axon of neocortical pyramidal neurons. Proc Natl Acad Sci U S A 95:5323-5328.

101.   McAdams CJ, Maunsell JHR (1999) Effects of attention on orientation-tuning functions of single neurons in macaque cortical area V4. J Neurosci 19:431-441.

102.   Mccarley RW, Faux SF, Shenton ME, Nestor PG, Adams J (1991) Event-related potentials in schizophrenia - their biological and clin correlates and a new model of schizophrenic Pathophysiology. Schizophr Res 4:209-231.

103.   McCormick DA, Shu YS, Hasenstaub A, Sanchez-Vives M, Badoual M, Bal T (2003) Persistent cortical activity: mechanisms of generation and effects on neuronal excitability. Cereb Cortex 13:1219-1231.

104.   Meador KJ, Ray PG, Echauz JR, Loring DW, Vachtsevanos GJ (2002) Gamma coherence and conscious perception. Neurology 59:847-854.

105.   Menendez RGD, Andino SLG (2000) Discussing the capabilities of Laplacian Minimization. Brain Topogr 13:97-104.

106.   Miller EK, Cohen JD (2001) An integrative theory of prefrontal cortex function. Annu Rev Neurosci 24:167-202.

107.   Miltner WH, Braun C, Arnold M, Witte H, Taub E (1999) Coherence of gamma-band EEG activity as a basis for associative learning. Nature 397:434-436.

108.   Mima T, Matsuoka T, Hallett M (2000) Functional coupling of human right and left cortical motor areas demonstrated with partial coherence analysis. Neurosci Lett 287:93-96.

109.   Mima T, Simpkins N, Oluwatimilehin T, Hallett M (1999) Force level modulates human cortical oscillatory activities. Neurosci Lett 275:77-80.

110.   Morf M, Vieira A, Lee DTL, Kailath T (1978) Recursive multichannel maximum entropy spectral estimation. IEEE Trans Geosci and Remote 16:85-94.

111.   Morrell LK, Morrell F (1966) Evoked potentials and reaction times: a study of intra-individual variability. Electroencephalogr Clin Neurophysiol 20:567-575.

112.   Murthy VN, Fetz EE (1992) Coherent 25- to 35-Hz oscillations in the sensorimotor cortex of awake behaving monkeys. Proc Natl Acad Sci U S A 89:5670-5674.

113.   Murthy VN, Fetz EE (1996) Oscillatory activity in sensorimotor cortex of awake monkeys: synchronization of local field potentials and relation to behavior. J Neurophysiol 76:3949-3967.

114.   Nakajima Y, Imamura N (2000) Relationships between attention effects and intensity effects on the cognitive N140 and P300 components of somatosensory ERPs. Clin Neurophysiol 111:1711-1718.

115.   Nichols TE, Holmes AP (2002) Nonparametric permutation tests for functional neuroimaging: a primer with examples. Hum Brain Mapp 15:1-25.

116.   Nikouline VV, Wikstrom H, Linkenkaer-Hansen K, Kesaniemi M, Ilmoniemi RJ, Huttunen J (2000) Somatosensory evoked magnetic fields: relation to pre-stimulus mu rhythm. Clin Neurophysiol 111:1227-1233.

117.   Nunez A, Garciaustt E, Buno W (1987) Intracellular theta-rhythm generation in identified hippocampal pyramids. Brain Res 416:289-300.

118.   Nunez PL, Wingeier BM, Silberstein RB (2001) Spatial-temporal structures of human alpha rhythms: theory, microcurrent sources, multiscale measurements, and global binding of local networks. Hum Brain Mapp 13:125-164.

119.   Nunez PL, Srinivasan R, Westdorp AF, Wijesinghe RS, Tucker DM, Silberstein RB, Cadusch PJ (1997) EEG coherency. I: statistics, reference electrode, volume conduction, Laplacians, cortical imaging, and interpretation at multiple scales. Electroencephalogr Clin Neurophysiol 103:499-515.

120.   Nunez PL, Silberstein RB, Shi Z, Carpenter MR, Srinivasan R, Tucker DM, Doran SM, Cadusch PJ, Wijesinghe RS (1999) EEG coherency II: experimental comparisons of multiple measures. Clin Neurophysiol 110:469-486.

121.   Oberman LM, Hubbard EM, McCleery JP, Altschuler EL, Ramachandran VS, Pineda JA (2005) EEG evidence for mirror neuron dysfunction in autism spectrum disorders. Cogn Brain Res 24:190-198.

122.   Palva S, Palva JM (2007) New vistas for alpha-frequency band oscillations. Trends Neurosci 30:150-158.

123.   Palva S, Linkenkaer-Hansen K, Naatanen R, Palva JM (2005) Early neural correlates of conscious somatosensory perception. J Neurosci 25:5248-5258.

124.   Perrin F, Bertrand O, Pernier J (1987) Scalp current-density mapping - value and estimation from potential data. IEEE Trans Biomed Eng 34:283-288.

125.   Petersen CCH (2002) Short-term dynamics of synaptic transmission within the excitatory neuronal network of rat layer 4 barrel cortex. J Neurophysiol 87:2904-2914.

126.   Petersen CCH, Hahn TTG, Mehta M, Grinvald A, Sakmann B (2003) Interaction of sensory responses with spontaneous depolarization in layer 2/3 barrel cortex. Proc Natl Acad Sci U S A 100:13638-13643.

127.   Pfurtscheller G, Stancak A, Jr., Neuper C (1996a) Post-movement beta synchronization. A correlate of an idling motor area? Electroencephalogr Clin Neurophysiol 98:281-293.

128. Pfurtscheller G, Stancak A, Jr., Neuper C (1996b) Event-related synchronization (ERS) in the alpha band--an electrophysiological correlate of cortical idling: a review. Int J Psychophysiol 24:39-46.

129. Pfurtscheller G, Stancak A, Jr., Edlinger G (1997a) On the existence of different types of central beta rhythms below 30 Hz. Electroencephalogr Clin Neurophysiol 102:316-325.

130. Pfurtscheller G, Neuper C, Andrew C, Edlinger G (1997b) Foot and hand area mu rhythms. Int J Psychophysiol 26:121-135.

131. Pineda JA (2005) The functional significance of mu rhythms: translating "seeing" and "hearing" into "doing". Brain Res Brain Res Rev 50:57-68.

132. Pineda JA, Allison BZ, Vankov A (2000) The effects of self-movement, observation, and imagination on mu rhythms and readiness potentials (RP's): toward a brain-computer interface (BCI). IEEE Trans Rehabil Eng 8:219-222.

133. Pineda JOA, Oberman LM (2006) What goads cigarette smokers to smoke? Neural adaptation and the mirror neuron system. Brain Res 1121:128-135.

134. Ploner M, Gross J, Timmermann L, Pollok B, Schnitzler A (2006) Oscillatory activity reflects the excitability of the human somatosensory system. Neuroimage 32:1231-1236.

135. Pollok B, Gross J, Muller K, Aschersleben G, Schnitzler A (2005) The cerebral oscillatory network associated with auditorily paced finger movements. Neuroimage 24:646-655.

136. Posner MI, Petersen SE (1990) The Attention System of the Human Brain. Annu Rev Neurosci 13:25-42.

137. Rahn E, Basar E (1993) Enhancement of Visual-Evoked Potentials by Stimulation during Low Prestimulus EEG Stages. Int J Neurosci 72:123-136.

138. Ray PG, Meador KJ, Smith JR, Wheless JW, Sittenfeld M, Clifton GL (1999) Physiology of perception - Cortical stimulation and recording in humans. Neurology 52:1044-1049.

139. Ray WJ, Cole HW (1985) EEG alpha activity reflects attentional demands, and beta activity reflects emotional and cognitive processes. Science 228:750-752.

140. Reyes A, Lujan R, Rozov A, Burnashev N, Somogyi P, Sakmann B (1998) Target-cell-specific facilitation and depression in neocortical circuits. Nat Neurosci 1:279-285.

141. Reynolds JH, Pasternak T, Desimone R (2000) Attention increases sensitivity of V4 neurons. Neuron 26:703-714.

142. Ritter P, Villringer A (2006) Simultaneous EEG-fMRI. Neurosci and Biobehav Rev 30:823-838.

143. Rodriguez E, George N, Lachaux JP, Martinerie J, Renault B, Varela FJ (1999) Perception's shadow: long-distance synchronization of human brain activity. Nature 397:430-433.

144. Rudolph M, Destexhe A (2001) Do neocortical pyramidal neurons display stochastic resonance? J Comput Neurosci 11:19-42.

145. Salenius S, Schnitzler A, Salmelin R, Jousmaki V, Hari R (1997) Modulation of human cortical rolandic rhythms during natural sensorimotor tasks. Neuroimage 5:221-228.

146. Salin PA, Bullier J (1995) Corticocortical connections in the visual-system - structure and function. Physiol Rev 75:107-154.

147. Salmelin R, Hari R (1994) Spatiotemporal characteristics of sensorimotor neuromagnetic rhythms related to thumb movement. Neuroscience 60:537-550.

148. Salmelin R, Hamalainen M, Kajola M, Hari R (1995) Functional segregation of movement-related rhythmic activity in the human brain. Neuroimage 2:237-243.

149. Sanes JN, Donoghue JP (1993) Oscillations in local field potentials of the primate motor cortex during voluntary movement. Proc Natl Acad Sci U S A 90:4470-4474.

150. Sauseng P, Klimesch W, Doppelmayr M, Pecherstorfer T, Freunberger R, Hanslmayr S (2005a) EEG alpha synchronization and functional coupling during top-down processing in a working memory task. Hum Brain Mapp 26:148-155.

151. Sauseng P, Klimesch W, Stadler W, Schabus M, Doppelmayr M, Hanslmayr S, Gruber WR, Birbaumer N (2005b) A shift of visual spatial attention is selectively associated with human EEG alpha activity. Eur J Neurosci 22:2917-2926.

152. Schaefer AT, Angelo K, Spors H, Margrie TW (2006) Neuronal oscillations enhance stimulus discrimination by ensuring action potential precision. Plos Biol 4:1010-1024.

153. Schubert R, Blankenburg F, Lemm S, Villringer A, Curio G (2006) Now you feel it - now you don't: ERP correlates of somatosensory awareness. Psychophysiology 43:31-40.

154. Serrien DJ, Pogosyan AH, Cassidy MJ, Brown P (2004) Anticipatory cortico-cortical interactions: switching the task configuration between effectors. Exp Brain Res 154:359-367.

155. Shu YS, Hasenstaub A, Badoual M, Bal T, McCormick DA (2003) Barrages of synaptic activity control the gain and sensitivity of cortical neurons. J Neurosci 23:10388-10401.

156. Silva LR, Amitai Y, Connors BW (1991) Intrinsic oscillations of neocortex generated by layer-5 pyramidal neurons. Science 251:432-435.

157. Simoes C, Salenius S, Curio G (2004) Short-term (approximate to 600 ms) prediction of perturbation dynamics for 10-and 20-Hz MEG rhythms in human primary sensorimotor hand cortices. Neuroimage 22:387-393.

158. Smith AT, Singh KD, Greenlee MW (2000) Attentional suppression of activity in the human visual cortex. Neuroreport 11:271-277.

159. Staines WR, Graham SJ, Black SE, McIlroy WE (2002) Task-relevant modulation of contralateral and ipsilateral primary somatosensory cortex and the role of a prefrontal-cortical sensory gating system. Neuroimage 15:190-199.

160. Stocks NG, Mannella R (2001) Generic noise-enhanced coding in neuronal arrays. Phys Rev E Stat Nonlin Soft Matter Phys 64:030902(1– 4).

161. Super H, van der Togt C, Spekreijse H, Lamme VAF (2003) Internal state of monkey primary visual cortex (V1) predicts figure-ground perception. J Neurosci 23:3407-3414.

162. Taylor-Clarke M, Kennett S, Haggard P (2002) Vision modulates somatosensory cortical processing. Curr Biol 12:233-236.

163. Thomson DJ (1982) Spectrum estimation and harmonic-analysis. Proc IEEE 70:1055-1096.

164. Tomberg C, Desmedt JE (1996) Non-averaged human brain potentials in somatic attention: the short-latency cognition-related P-40 component. J Physiol (Lond) 496:559-574.

165. Tomberg C, Desmedt JE, Ozaki I, Nguyen TH, Chalklin V (1989) Mapping somatosensory evoked-potentials to finger stimulation at intervals of 450 to 4000 msec and the issue of habituation when assessing early cognitive components. Electroencephalogr Clin Neurophysiol 74:347-358.

166. Tsodyks M, Kenet T, Grinvald A, Arieli A (1999) Linking spontaneous activity of single cortical neurons and the underlying functional architecture. Science 286:1943-1946.

167. Vanessen DC, Gallant JL (1994) Neural mechanisms of form and motion processing in the primate visual-system. Neuron 13:1-10.

168. Vanrotterdam A, Dasilva FHL, Vandenende J, Viergever MA, Hermans AJ (1982) A model of the spatial-temporal characteristics of the alpha-rhythm. Bull Math Biol 44:283-305.

169. Varela F, Lachaux JP, Rodriguez E, Martinerie J (2001) The brainweb: phase synchronization and large-scale integration. Nat Rev Neurosci 2:229-239.

170. Vertes RP (2005) Hippocampal theta rhythm: a tag for short-term memory. Hippocampus 15:923-935.

171. von Stein A, Chiang C, Konig P (2000) Top-down processing mediated by interareal synchronization. Proc Natl Acad Sci U S A 97:14748-14753.

172.   Waberski TD, Gobbele R, Darvas F, Schmitz S, Buchner H (2002) Spatiotemporal imaging of electrical activity related to attention to somatosensory stimulation. Neuroimage 17:1347-1357.

173.   Wiesenfeld K, Moss F (1995) Stochastic resonance and the benefits of noise - from ice ages to crayfish and squids. Nature 373:33-36.

174.   Wiest MC, Nicolelis MAL (2003) Behavioral detection of tactile stimuli during 7–12 Hz cortical oscillations in awake rats. Nat Neurosci 6:913-914.

175.   Wikstrom H, Huttunen J, Korvenoja A, Virtanen J, Salonen O, Aronen H, Ilmoniemi RJ (1996) Effects of interstimulus interval on somatosensory evoked magnetic fields (SEFs): a hypothesis concerning SEF generation at the primary sensorimotor cortex. Evoked Potentials-Electroencephalogr Clin Neurophysiol 100:479-487.

176.   Winterer G, Ziller M, Dorn H, Frick K, Mulert C, Dahhan N, Herrmann WM, Coppola R (1999) Cortical activation, signal-to-noise ratio and stochastic resonance during information processing in man. Clin Neurophysiol 110:1193-1203.

177.   Yamagishi N, Callan DE, Goda N, Anderson SJ, Yoshida Y, Kawato M (2003) Attentional modulation of oscillatory activity in human visual cortex. Neuroimage 20:98-113.

178.   Zucker RS, Regehr WG (2002) Short-term synaptic plasticity. Annu Rev Physiol 64:355-405.

BIOGRAPHAICAL SKETCH

Yan Zhang received her Bachelor of Engineering from Xi'an Institute of Technology in 1996. After receiving top academic records through examination, she became a graduate student in the Department of Electronics in the College of Information Science at the Beijing Normal University, majoring in nonlinear system and data processing. After completing her master's degree in 1999, she stayed at the Beijing Normal University and worked as a college teacher and a researcher. In 2003, she became a PhD student in Center for Complex Systems and Brain Sciences at the Florida Atlantic University. In 2004, she was awarded an Alumni Fellowship for graduate study in biomedical engineering at University of Florida. Her research interests are biomedical signal processing, sensory perception, attention control and human motor control. She completed a Doctorate in Philosophy in August of 2008 specializing in neuroinformatics. Yan Zhang is currently a member of Society of Neuroscience and Institute of Electrical and Electronics Engineers.